




Cite this: *RSC Adv.*, 2025, **15**, 21582

# Photothermal applications of upconversion nanoparticles

Masoomah Amoozadeh,<sup>a</sup> Danial Khorsandi,<sup>b</sup> Amin Farahani,<sup>c</sup> Atefeh Zarepour,<sup>d</sup> Arezoo Khosravi,<sup>ef</sup> Siavash Iravani  <sup>\*g</sup> and Ali Zarrabi  <sup>\*h</sup>

Upconversion nanoparticles (UCNPs) have become a versatile nanoplatform with promising potential in photothermal applications. By efficiently converting near-infrared (NIR) light into heat, UCNPs offer a non-invasive approach to induce hyperthermia in specific target tissues, such as cancer cells, while preserving surrounding healthy cells. The utilization of UCNPs in combination therapies, multifunctional nanosystems, and regenerative medicine applications highlights their versatility and adaptability in addressing complex healthcare challenges. By leveraging the multifunctionality of UCNPs, researchers can develop approaches for disease management, drug delivery, and monitoring, opening the path for more effective and tailored biomedical interventions. However, challenges such as NIR light penetration limitations, biocompatibility considerations, photothermal conversion efficiency optimization, tumor targeting strategies, and clinical translation studies need to be carefully considered and overcome to maximize the efficacy of UCNPs in photothermal applications. We aim to provide an inclusive exploration of the potential applications of UCNPs in photothermal therapy, highlighting their unique properties and versatility in targeted therapeutic interventions. This review explores the photothermal conversion efficiency, tumor-targeting strategies, and future prospects of UCNPs, aiming to highlight the challenges and opportunities in employing these nanoparticles for precise and effective applications in cancer therapy, tissue engineering, and personalized medicine.

Received 2nd April 2025  
Accepted 12th June 2025

DOI: 10.1039/d5ra02303c

rsc.li/rsc-advances

## 1 Introduction

Upconversion nanoparticles (UCNPs) have attracted significant interest in photothermal applications due to their unique ability to convert near-infrared (NIR) light into higher-energy visible or ultraviolet light, a process known as upconversion.<sup>1,2</sup> This property makes UCNPs promising candidates for various photothermal therapies and imaging techniques. One of the most promising applications of UCNPs is in precision cancer therapy. Through functionalization of UCNPs with targeting agents, they could be directed to the specific tumor sites.<sup>3,4</sup> Upon exposure to NIR light, UCNPs produce heat, which leads

to localized hyperthermia that selectively eliminates cancer cells while preserving healthy tissue. This targeted photothermal therapy (PTT) holds great promise for improving treatment outcomes while minimizing side effects. PTT is an innovative cancer treatment that involves injecting materials with high photothermal conversion efficiency into the body, where they accumulate near tumor tissues. Upon irradiation with an external light source, these materials convert the absorbed light energy into heat, effectively raising the temperature to kill tumor cells while minimizing damage to surrounding healthy tissues. This targeted approach offers a minimally invasive and precise method for cancer therapy by leveraging the localized heating effect generated through photothermal conversion.<sup>5</sup> Photothermal conversion is an efficient method of harnessing solar energy by converting light into heat through three main mechanisms: plasmonic localized heating, where metal nanostructures generate heat *via* electron oscillations; non-radiative relaxation, where excited electrons in semiconductors release energy as heat without emitting light; and thermal vibration, involving the conversion of absorbed light into molecular or lattice vibrations that produce heat. These processes enable various applications such as solar energy harvesting, photothermal therapy, and water purification by effectively transforming electromagnetic radiation into thermal energy.<sup>6</sup> UCNPs are also developing the field of

<sup>a</sup>Department of Chemistry, University of Isfahan, Isfahan 81746, Iran

<sup>b</sup>Terasaki Institute for Biomedical Innovation, Woodland Hills CA, 91367, USA

<sup>c</sup>Cellular & Molecular Endocrine Research Center, Research Institute for Endocrine Sciences, Shahid Beheshti University of Medical Sciences, Tehran, Iran

<sup>d</sup>Department of Biology, Faculty of Arts and Sciences, Kocaeli University, 41001, İzmit, Kocaeli, Türkiye

<sup>e</sup>Department of Genetics and Bioengineering, Faculty of Engineering and Natural Sciences, Istanbul Okan University, Istanbul 34959, Türkiye

<sup>f</sup>Graduate School of Biotechnology and Bioengineering, Yuan Ze University, Taoyuan 320315, Taiwan

<sup>g</sup>Independent Researcher, W Nazar ST, Boostan Ave, Isfahan, Iran. E-mail: siavashira@gmail.com

<sup>h</sup>Department of Biomedical Engineering, Faculty of Engineering and Natural Sciences, Istinye University, Istanbul 34396, Türkiye. E-mail: alizarrabi@gmail.com


photothermal imaging. By utilizing UCNPs as contrast agents, researchers can visualize temperature changes with exceptional spatial resolution in biological tissues. This real-time monitoring of heat generation provides valuable insights into disease progression, drug delivery efficiency, and tissue responses to treatment, making it a powerful tool in biomedical research and diagnostics.<sup>3,7–9</sup>

In addition to their use in photothermal monotherapy, UCNPs are being integrated into multimodal therapeutic approaches.<sup>10</sup> By combining photothermal treatment with chemotherapy, immunotherapy, photodynamic therapy (PDT), or other modalities, synergistic effects can be harnessed to enhance therapeutic outcomes. UCNPs play a pivotal role in these combinatorial therapies by improving drug delivery, enhancing immune responses, and optimizing treatment efficacy.<sup>11</sup> They were studied for their immunomodulatory effects when used in combination with immunotherapy. By leveraging the photothermal properties of UCNPs to stimulate immune responses, researchers can enhance the body's natural defense mechanisms against cancer cells. This multimodal approach not only could target tumors directly but also could enhance the immune system's ability to recognize and eliminate cancer cells, leading to more effective and sustained antitumor effects. In addition, multimodal therapeutic strategies with UCNPs hold promise in the field of precision medicine. By tailoring treatment regimens to individual patients based on their unique disease characteristics and genetic profiles, clinicians could enhance therapeutic results while reducing adverse

effects. UCNPs are essential in this personalized approach, providing accurate and effective transfer of therapeutic agents to affected tissues.<sup>10,12,13</sup>

In PTT using UCNPs, the nanoparticles (NPs) are functionalized with targeting agents to enable selective accumulation at tumor sites (Fig. 1).<sup>14</sup> Upon exposure to NIR light, UCNPs effectively transform light energy into heat, resulting in localized hyperthermia in the tumor microenvironment.<sup>15</sup> This targeted approach allows for the selective destruction of cancer cells while minimizing damage to healthy tissues, offering a more effective and less invasive treatment option for various types of cancer. UCNPs exhibit excellent photothermal conversion efficiency, meaning they can efficiently convert NIR light into heat. This property enables precise control over the amount of heat generated in the target tissue, allowing treatment regimens to be tailored to the specific characteristics of the tumor. By adjusting the intensity and duration of NIR light exposure, clinicians can optimize the therapeutic outcome and reduce side effects of conventional cancer treatments. In addition to cancer treatment, PTT with UCNPs can be utilized for real-time monitoring and imaging of the treatment process. By incorporating UCNPs as contrast agents of different imaging modalities, researchers can observe the distribution of NPs in the body and monitor thermal changes in the target tissue during therapy. This imaging modality provides valuable feedback on the efficacy of the treatment and allows for adjustments to be made in real-time, enhancing treatment precision and patient outcomes.<sup>15–17</sup>

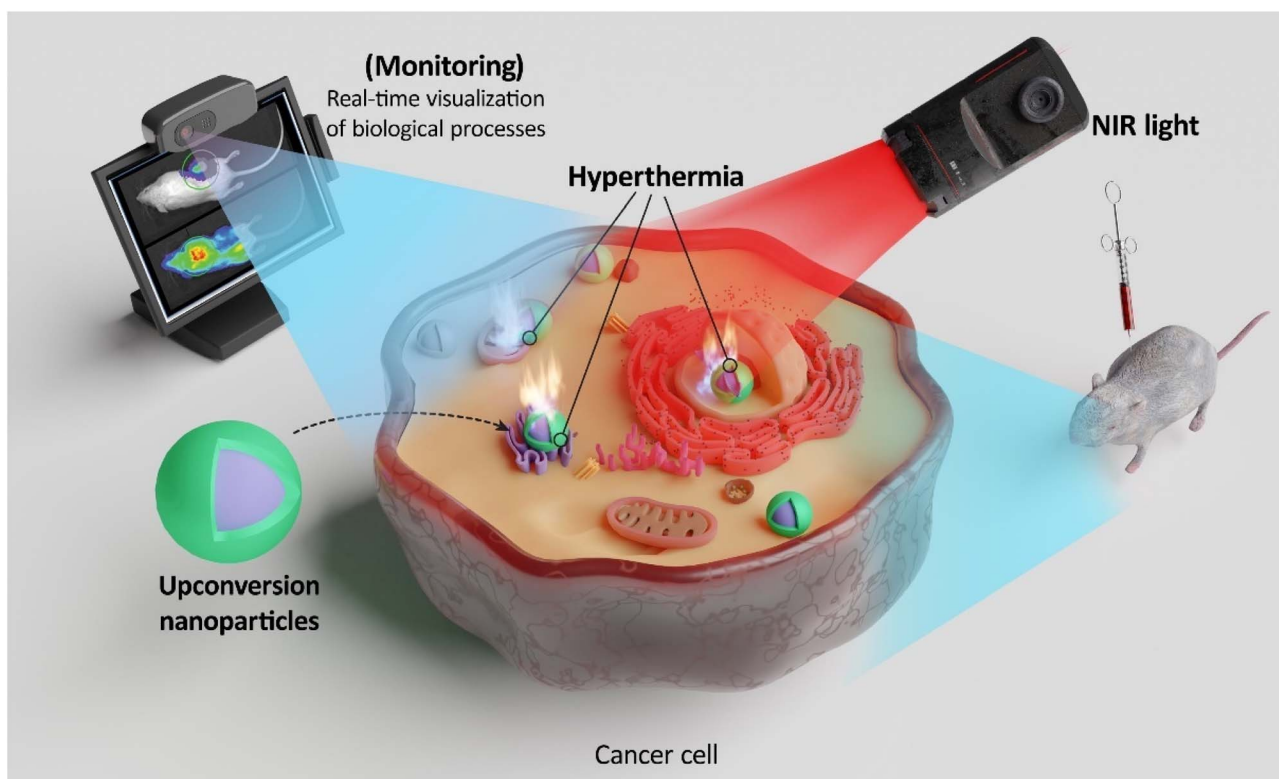


Fig. 1 Application of upconversion nanoparticles for photothermal therapy and imaging applications.

Imaging-guided therapy incorporating UCNPs represents an advanced approach in precision medicine, offering simultaneous diagnostic imaging and targeted therapeutic interventions.<sup>8,18</sup> UCNPs play a central role in this approach, acting as versatile contrast agents for imaging techniques such as fluorescence imaging, photoacoustic imaging, and computed tomography (CT), while also enabling targeted therapy delivery.<sup>19</sup> A major benefit of UCNPs in imaging-guided therapy is their capacity to deliver high-resolution, real-time imaging of diseased tissues. By functionalizing UCNPs with specific targeting ligands, researchers can direct these NPs to disease sites and visualize them using various imaging techniques. This precise imaging allows for early detection, accurate localization, and monitoring of disease progression, thereby supporting personalized treatment strategies and improved patient outcomes. UCNPs can be customized to carry therapeutic agents and target specific cells or tissues, allowing for precise drug delivery and localized therapy. In imaging-guided therapy, UCNPs could be acted as both imaging contrast agents and drug carriers, allowing clinicians to visualize the accumulation of NPs in target areas and monitor the release of therapeutic payloads. This targeted method reduces unintended effects and improves the treatment efficacy. Researchers can track the distribution of UCNPs, assess the uptake of therapeutic agents, and visualize changes in tissue characteristics during therapy. This dynamic feedback loop allows for the real-time adjustments to treatment parameters, ensuring optimal therapeutic outcomes and enhanced patient safety.<sup>9,18,20</sup>

The integration of UCNPs and PTT in tissue engineering offers significant potential for progressing regenerative medicine and tissue repair strategies.<sup>21</sup> By combining the unique properties of UCNPs for imaging and therapeutic applications with the targeted heat generation capabilities of PTT, researchers are exploring innovative approaches to enhance tissue regeneration, scaffold design, and therapeutic delivery in tissue engineering.<sup>22</sup> UCNPs offer exceptional imaging capabilities, allowing for high-resolution visualization of tissue structures, cell behavior, and biomaterial interactions in real time. By incorporating UCNPs into tissue engineering constructs, researchers can monitor cell migration, proliferation, and differentiation, offering valuable insights into the dynamics of tissue regeneration.<sup>8,18,22</sup> Moreover, the photothermal properties of UCNPs enable localized heat generation through PTT, which can be harnessed to stimulate cellular responses, promote tissue growth, and improve the integration of biomaterial scaffolds with host tissues.<sup>23</sup> The combination of UCNPs and PTT in tissue engineering provides researchers with a powerful tool to modulate the tissue microenvironment in a controlled and spatially precise manner.<sup>22,24</sup> By selectively activating UCNPs in specific regions of the engineered tissue, researchers can induce localized heating, alter cellular behavior, and create gradients of biological signals to guide tissue development.<sup>22,24</sup> This level of precision offers new opportunities for designing complex tissue constructs with tailored properties and functionalities. UCNPs can also act as carriers for therapeutic agents in tissue engineering applications, allowing for targeted drug delivery and controlled release within the engineered tissue. By

functionalizing UCNPs with bioactive molecules or growth factors, researchers can improve the regenerative potential of tissue constructs and promote specific cellular responses. When combined with PTT, UCNPs can facilitate on-demand drug release and localized treatment, further improving the therapeutic outcomes in tissue engineering applications.<sup>22,24</sup>

This review aims to comprehensively examine the photothermal applications of UCNPs in tissue engineering, imaging-guided therapy, and targeted cancer therapy, highlighting their potential in advancing personalized medicine and precision healthcare. This review examines the synergistic effects of UCNPs and PTT in targeted cancer treatment through localized hyperthermia, addressing challenges in treatment optimization and the potential for personalized therapeutic strategies. By examining the integration of UCNPs and PTT in tissue engineering, challenges such as biocompatibility, long-term stability, and clinical translation are addressed, while future perspectives focus on optimizing UCNP design for enhanced regenerative strategies. In imaging-guided therapy, the emphasis is on employing UCNPs for precise diagnostic imaging and targeted therapeutic delivery, with a vision for real-time treatment monitoring and personalized treatment regimens. Future perspectives encompass the exploration of novel therapeutic approaches, advancements in imaging modalities, and the translation of UCNPs and PTT into clinical settings, aiming to develop tissue engineering, imaging-guided therapy, and cancer treatment paradigms.

## 2 Photothermal therapy using UCNPs

### 2.1 Principals and mechanisms of photothermal therapy

PTT represents a novel therapeutic approach that uses localized hyperthermia to treat different types of diseases. It is based on the injection of photothermal agent into the target tissue and exposing it to light for a predetermined duration, resulting in a localized temperature increase. Regarding the human body, any increase in body temperature beyond the 37 °C is considered as an abnormal state and indicates as fever. In some cases, this can cause irreversible tissue or organ damage, and eventually causes organ failure.<sup>25</sup> The first indication of the therapeutic benefits of thermal therapy occurred in 19th century. The cancer patient experienced a fever after receiving living bacteria that caused a partial regression of the tumor tissue. Around the same time, circulating hot water was successfully used to treat uterine cervical cancer.<sup>26</sup> For many years, treatment options for cancer patients were limited to surgery, radiation therapy, and chemotherapy, alone or in combination form. However, the limitations of these traditional therapies—from adverse side effects to insufficient efficacy against metastatic tumors—led to the introduction of novel therapeutic methods among them is thermal therapy.<sup>27,28</sup> From then on, a new age of thermal therapy for cancer treatment began, and it was eventually adopted as a method for treating several other illnesses as well.<sup>29</sup> The technological advantage has driven a shift in the design of modern PTT platforms toward multifunctional nanomaterials capable of both treatment and real-time monitoring. NP induce PTT is a type of these new methods that is based on the



injection of NPs with optimized photothermal conversion efficiency (PCE) to transduce light into thermal energy. These agents, upon systemic administration, are designed to particularly target and accumulate near tumor sites. Illumination by external NIR source starts the absorption of photons by the NPs and converting them into the localized heat that leads to increasing the temperature within tumor microenvironment and so facilitating the eradication of targeted tumor cells (Fig. 2).<sup>30</sup>

The thermal properties of NPs, their target accumulation, and the intensity of applied light are essential for controlling the PTT performance. Necrosis and apoptosis are the primary mechanisms of cells treated by PTT. Necrosis results in the loss of plasma membrane integrity and the release of damage-associated molecular patterns (DAMPs) into the surrounding tissue that can trigger harmful inflammatory reactions, making necrosis an unfavorable outcome. By contrast, apoptosis maintains membrane integrity and signals for phagocytosis without causing inflammation. However, it should be noted that when cells lose membrane integrity and release DAMPs but do not initiate phagocytosis, an apoptotic process can transition to secondary necrosis.<sup>31,32</sup> The main challenge in PTT is to

protect healthy tissues adjacent to the tumor from collateral thermal damage. To ensure precise energy deposition, the laser parameters such as wavelength and power must be optimized together with the design of an applicator. In addition, to perform targeted ablation, it is necessary to maintain tumor tissue temperature within therapeutic limits while taking into account the physical and optical characteristics of tissues.<sup>33</sup>

To achieve this precision, two main strategies are employed: accumulating photosensitizers inside the targeted site using targeting agent and utilizing low-temperature techniques. Li *et al.*, use of Lyp-1 ligands targets overexpressed p-32 protein in breast cancer cells. With this technique, the concentration of therapeutic drugs inside the tumor was increased and the exposure to healthy tissues was decreased since the NPs were more likely to adhere to and be absorbed by the cancer cells.<sup>34</sup> They used gambogic acid (GA) in PEGylated 1D metal organic frameworks (MOFs) to inhibit the synthesis of heat shock proteins (HSPs), particularly HSP90. This inhibition reduced the thermal resistance of tumor cells, providing efficient PTT at lower temperature and thus reducing the risk of incidental heat damage.<sup>35</sup> Similarly, Shao *et al.* applied the HSP90 inhibitor SNX-2112 on a graphene-based nanoplatform, demonstrating

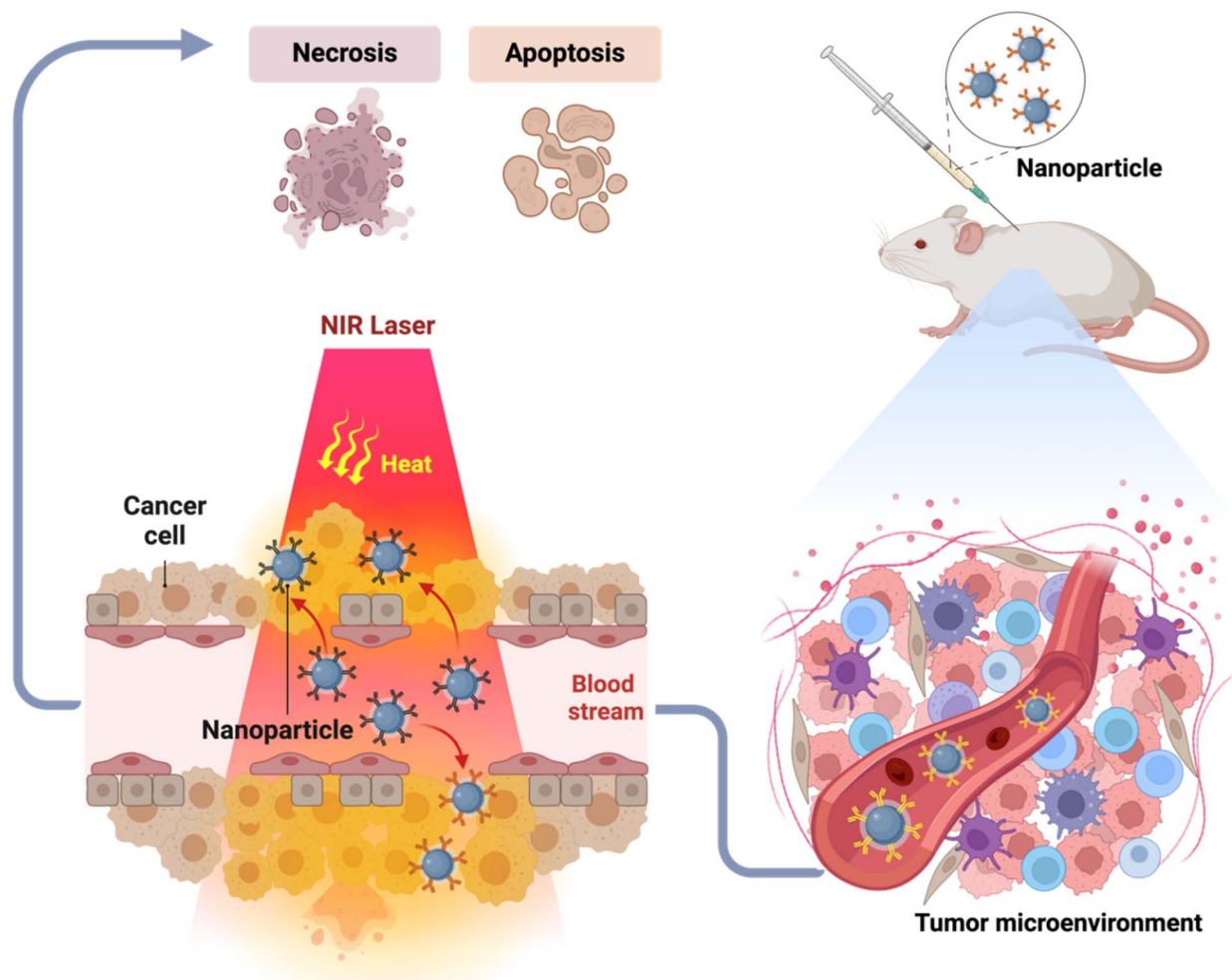


Fig. 2 Schematic illustration of PTT process. Created by <https://www.biorender.com>.



that low-temperature PTT could induce autophagic cell death in tumor cells. On the other hand, it could activate the immune system, contributing to long-term tumor suppression.<sup>36</sup>

Another key factor in maximizing therapeutic results in PTT is the choice of laser, either in pulse or continuous mode. The desired degree of heat damage and the anticipated depth of tissue penetration must be considered while choosing laser mode. Using high-power lasers—typically >100 W—the pulse mode delivers energy in bursts to raise the temperature of tumor tissue and cause irreversible damage. In contrast, the continuous mode maintains a steady laser exposure, with the duration adjusted according to the laser's power to achieve the desired thermal effect without harming surrounding tissues.<sup>37</sup> Historically, the clinical application of laser radiation in the visible range was limited due to its strong absorption by human tissues. The emergence of NIR lasers, calibrated to operate within special biological windows (the  $\lambda \approx 650\text{--}1064\text{ nm}$ ), has significantly advanced PTT. These biological windows include the first window (NIR-I, 650–950 nm) and the second window (NIR-II, 1000–1350 nm), both characterized by reduced absorption by water and hemoglobin, thereby enhancing tissue transparency and enabling deeper laser penetration.<sup>38</sup>

In the absence of targeted photothermal agents, PTT lacks selectivity, potentially damaging both tumor and healthy cells. Particularly in cases where the target cancer tissue is located into the deeper part of body, it may damage protective tissues. To mitigate such risks, it is essential to employ agents that can enhance the light absorption of cancer cells and so protecting the surrounding healthy cells.<sup>32</sup>

## 2.2 Commercially available photothermal therapy agents

As the clinical and preclinical perspective, several PTT agents have been developed and evaluated for cancer treatment and other biomedical applications. These agents vary in terms of chemical composition, photothermal conversion efficiency, biocompatibility, and clinical trials. Nanomaterials with size between 1–100 nm are good candidates in this case. Through either active or passive mechanisms, NPs are internalized by the targeted cells. In passive targeting, the unique permeability of tumor vasculature allows NPs to accumulate within tumor areas *via* enhanced permeability and retention (EPR) effect. Physicochemical properties of NPs, such as shape, size, and surface charge, influence this process.<sup>39</sup> On the other hand, active targeting is achieved by biofunctionalizing NPs' surface with ligands, including small molecules, antibodies, peptides, or aptamers, specifically designed for high affinity to receptors overexpressed on the tumor cells. In addition, NPs encapsulated in cell membranes use the natural homing abilities of carrier cells such as red blood cells, T lymphocytes, macrophages and neutrophils to enhance tumor targeting.<sup>39,40</sup> This approach not only facilitates access to tumor sites but also uses biomimetic covering techniques to avoid the detection of antibodies and respond to the microenvironment's specific features, such as acidity or light. Furthermore, transcytosis provides a complementary mechanism, enabling NPs to traverse cellular barriers *via* vesicular transport across endothelial cells and facilitating

entry into tumor tissue.<sup>41</sup> Gold-based nanomaterials (*e.g.*, gold nanorods, nanocages, and nanoshells) are among the most extensively studied PTT agents due to their tunable surface plasmon resonance (SPR) in the near-infrared (NIR) region and high photothermal conversion efficiency. Gold nanorods, for instance, can efficiently absorb NIR light and convert it into localized heat.<sup>42</sup> However, their long-term retention in the body and lack of biodegradability raise safety concerns.<sup>43</sup> Moreover, their synthesis can be cost-prohibitive and sensitive to aggregation under physiological conditions.<sup>44</sup> Carbon-based nanomaterials, including graphene oxide, carbon nanotubes, and carbon dots, exhibit excellent NIR absorption and thermal stability. These materials offer high photothermal performance and can be functionally modified for enhanced tumor targeting.<sup>45</sup> Nonetheless, concerns remain regarding their biodegradability and long-term toxicity.<sup>46</sup> Copper sulfide (CuS) nanoparticles are another class of PTT agents with strong NIR absorbance and favorable biodegradability, that offer a cost-effective alternative to noble metals and demonstrate good photothermal stability. However, their photothermal conversion efficiency is generally lower than that of gold-based agents.<sup>47,48</sup> Polydopamine (PDA)-based nanoparticles have gained attention due to their strong photothermal effects and excellent biocompatibility. PDA mimics natural melanin and can be easily connected to other compounds, making it a versatile nanoplatform.<sup>49</sup> However, their moderate photothermal conversion efficiency (PCE) and performance degradation under repeated laser exposure may limit long-term application.<sup>50</sup> Indocyanine Green (ICG), a small-molecule dye FDA-approved for imaging, has also been utilized for clinical PTT due to its strong NIR absorption. However, ICG suffers from poor photostability, rapid degradation, and nonspecific biodistribution, which limit its therapeutic utility in long-term or deep-tissue applications.<sup>51,52</sup>

Each of these agents brings a unique set of capabilities and challenges. Their main important limitations are included poor biodegradability, suboptimal targeting, low thermal conversion at low doses, or systemic toxicity; highlight the need for next-generation PTT platforms. This creates a compelling rationale for the use of UCNPs, which offer multifunctionality, deep-tissue imaging, and potential for controlled heating and drug delivery.

## 2.3 Upconversion nanoparticles and photothermal therapy

UCNPs have emerged as promising agents in photothermal therapy (PTT) due to their unique ability to absorb low-energy near-infrared (NIR) light and emit higher-energy photons in the visible or ultraviolet (UV) range. Normally, UCNPs have three main components; the host matrix alongside the sensitizer (absorbing or donating) and activator (accepting or emitting) ions.<sup>53,54</sup> The luminescence process is driven by activator ions, which are supported by sensitizer ions that absorb near-infrared (NIR) light. These sensitizer ions are excited by the light source and efficiently transfer the absorbed energy to the activator ions, which then emit light.<sup>55</sup> The most commonly used matrix materials include fluorides, oxides, and sulfides.



Among these, fluorides are the most frequently utilized due to their larger band gap and lower phonon energy. The rare earth elements  $\text{Er}^{3+}$ ,  $\text{Tm}^{3+}$ ,  $\text{Ho}^{3+}$ , and  $\text{Eu}^{3+}$  are frequently employed as activators. They control the UCNPs' light emission to a significant extent. As an example, UCNPs doped with  $\text{Er}^{3+}$  glow green, but UCNPs doped with  $\text{Tm}^{3+}$  and  $\text{Ho}^{3+}$  fluoresce blue and red, respectively. Because of its wide absorption cross section and efficient energy transfer, the rare earth element  $\text{Yb}^{3+}$  is commonly used as a sensitizer for 980 nm-excited upconversion. However, the 980 nm wavelength significantly overlaps with the strong absorption band of water, which can cause local heating and tissue damage during biological applications. To overcome this limitation, recent developments have focused on 808 nm-excited UCNPs, using  $\text{Nd}^{3+}$  as an alternative sensitizer—often co-doped with  $\text{Yb}^{3+}$ —to reduce tissue heating while maintaining efficient upconversion. In addition, organic dyes are emerging as a novel class of sensitizers with promise upconversion luminescence (UCL) capabilities when combined with other reagents.<sup>56</sup> The efficiency of the upconversion process depends on selecting an appropriate host matrix, which influences the energy transfer dynamics between sensitizer and activator ions. To have an ideal host matrix material it needs to (i) integrating luminescent centers while preserving the crystalline architecture; (ii) having low phonon energy to decrease non-radiative losses (vital for improving quantum yield); (iii) being permeable to near-infrared photons, allowing for effective energy distribution within the matrix; and (iv) demonstrating chemical and thermal stability to maintain the crystallinity of the matrix.<sup>57–59</sup> To incorporating lanthanide absorbers and emitters, host matrices are categorized into two primary classifications: amorphous and crystalline.<sup>60</sup> Factors other than atomic size or spacing that ensure a homogeneous distribution of ions between emitters and absorbers influence the choice of an appropriate host matrix. The low phonon energy of the lattice is an important criterion that must be achieved to reduce the radiative loss and thereby improve its luminescence. In addition, even if the dopants remain the same, the specific interaction dynamics of the rare earth ions in the different lattices can significantly influence the upconversion emissions.<sup>61</sup>

Some of the UCNPs, especially those with optimized doping concentrations or specific host matrix, can generate heat directly upon NIR irradiation. This effect is related to the non-radiative relaxation processes, including multi-phonon relaxation and lattice vibrations, which convert absorbed photon energy into heat. This intrinsic photothermal conversion can be used to induce localized hyperthermia in cancerous tissues, leading to cell apoptosis or necrosis.<sup>62,63</sup> The integration of UCNPs into PTT not only addresses some of the limitations of the current available photothermal agents, but also enables advanced theranostic applications through simultaneous imaging and treatment. Unlike conventional photothermal agents that rely solely on heat generation upon NIR irradiation, UCNPs absorb low-energy NIR light and emit higher-energy visible or UV photons through nonlinear multiphoton processes. This property enables them to act simultaneously as deep-tissue imaging agents, localized heat sources, and

photoactivators for light-sensitive therapeutic compounds. Most traditional agents lack this level of spatiotemporal control and multi-functionality. Moreover, UCNPs exhibit sharp emission peaks, minimal autofluorescence interference, and excellent photostability, which are advantageous for real-time imaging and temperature monitoring during treatment. Their emission-based temperature sensitivity provides built-in feedback for controlled hyperthermia, an area where other inorganic agents typically require external thermometry.<sup>64–66</sup>

Another distinguishing factor is programmability. UCNPs can be doped and coated in modular architectures (e.g., core/shell structures) to tune both optical and thermal properties, or to co-load imaging/therapeutic agents. This makes them an ideal scaffold for theranostic platforms, particularly in combination therapies or where precise thermal dosing is critical. Therefore, while other inorganic nanomaterials offer high photothermal conversion or strong NIR absorption, UCNPs uniquely integrate diagnostic, therapeutic, and monitoring functionalities in a single nanopatform. These features justify their increasing use in advanced PTT systems, particularly for deep-tissue and image-guided therapies where conventional agents fall short.<sup>67</sup>

As mentioned before, during an upconversion process two or more photons must be absorbed by the NPs to give enough energy. In this context, five fundamental UC mechanisms (Fig. 3) exist including: (1) excited-state absorption (ESA): it shows the sequential absorption of excitation photons by a single ion through a three-level system, involving two consecutive photon absorptions. This process occurs because of the similar distances between G and E1 and E1 and E2, as well as the intermediate level E1's reservoir capacity. Due to the relatively long-lived nature of the E1 excited state, an ion that has reached this level is more likely to absorb an additional pump photon, enabling its transition to a higher excited state, E2. Upconverted emission from the E2 level will therefore happen. Lanthanide ions such as  $\text{Er}^{3+}$ ,  $\text{Tm}^{3+}$ , and  $\text{Ho}^{3+}$  exhibit a series of intrinsic, well-defined energy levels arranged in a ladder-like configuration. This inherent structure allows for the sequential absorption of multiple photons *via* ESA, a process essential for efficient upconversion luminescence. These ions are well-suited for the excitation wavelengths provided by commercially available diode lasers, typically around 975 and 808 nm,<sup>68</sup> (2) energy transfer upconversion (ETU) that operates through the interaction of adjacent ions, namely an activator and a sensitizer, facilitating energy transfer. The harvested photons are continually transferred to the excited state E1 of the activator by the sensitizer, which absorbs the pump photons and moves them from the ground state to the E1 energy level. Simultaneously, the sensitizer reverts to the ground state, allowing the activator to achieve the higher emission state, E2. The efficiency of ETU is influenced by the proximity between sensitizer and activator ions, as well as the ion concentration. ETU plays a crucial role in explaining the UCL mechanism in UCNPs.<sup>69,70</sup> (3) Cooperative sensitization upconversion (CSU) involves the interactions among two ions or between a pair of ions and an additional ion.<sup>71</sup> Cooperative upconversion and energy transfer upconversion share several



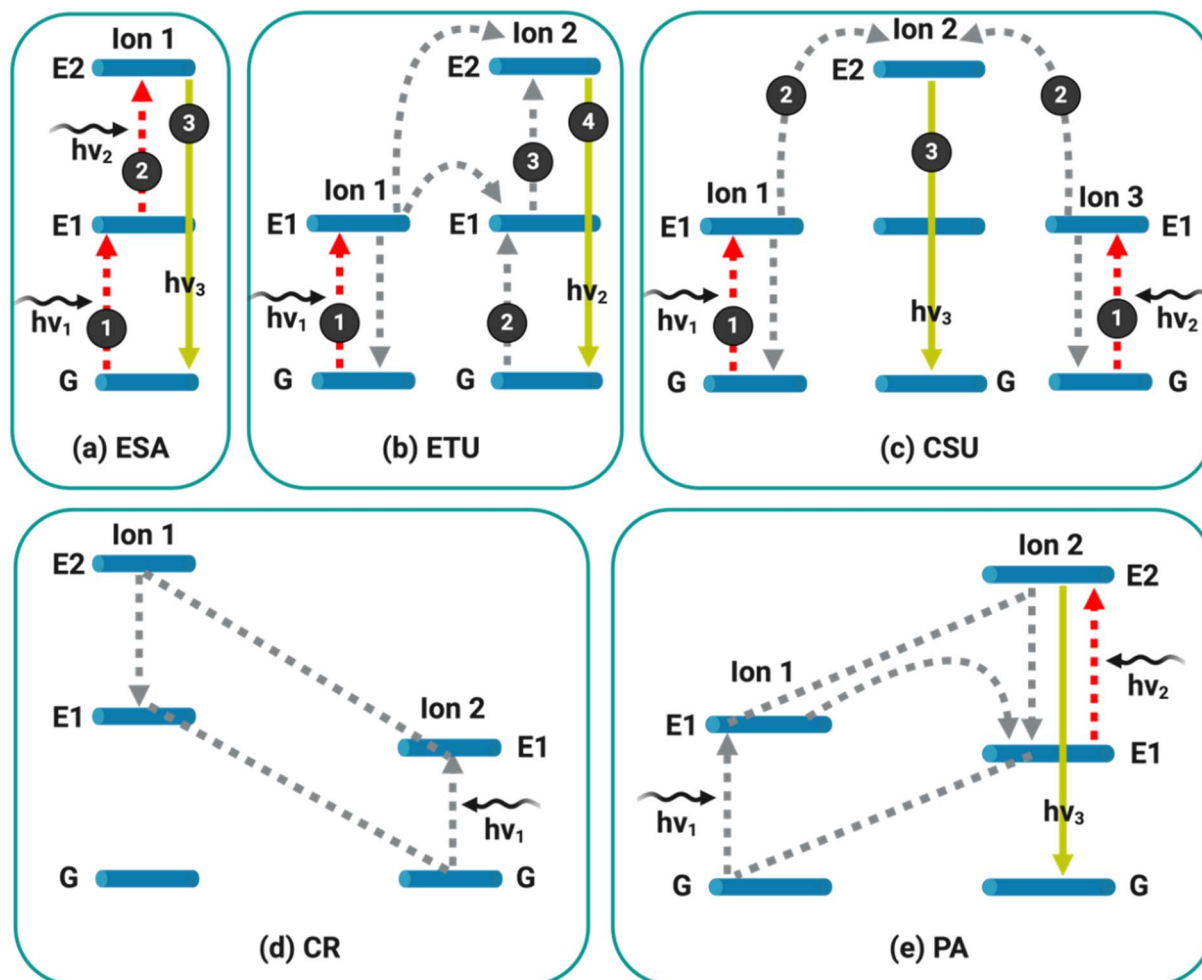


Fig. 3 Schematic illustration of upconversion mechanisms in UCNP. The diagram delineates the five primary pathways through which upconversion occurs: (a) Excited State Absorption (ESA), (b) Energy Transfer Upconversion (ETU), (c) Cooperative Sensitization Upconversion (CSU), (d) Cross-Relaxation (CR), and (e) Photon Avalanche (PA). The red line signifies photon excitation, illustrating the initial absorption of photons that elevates the energy state of the particles. The grey line represents energy transfer processes, where energy is transferred between ions within the UCNP matrix. The yellow line indicates emission processes, where the relaxation of ions to a lower energy state results in photon emission. Created by <https://www.biorender.com>.

theoretical similarities in their underlying mechanisms. When a photon with sufficient pump power excites ions 1 and 3 to the E1 energy level, dopant ion 2 is simultaneously elevated to a higher energy state (E1) through cooperative interactions. An upconverted photon is then emitted as ion 2 undergoes radiative relaxation back to the ground state. Although CSU and ETU are somewhat similar, CSU deals with quasi-virtual levels, which are theoretically explicable in terms of a higher-order disturbance.<sup>72,73</sup> (4) Cross-relaxation (CR) ion-ion interaction is the basic cause of cross-relaxation, which is the transfer of energy between two ions. During CR, an ion in the higher excited state transfers part of its energy to a neighboring ion in the ground state (G), leaving both ions in the intermediate state. Although CR is essential for fine-tuning the emission color of UCNP, it is also a principal cause of concentration-induced quenching.<sup>68</sup> (5) Photon avalanche (PA): The ESA and CR processes combine to form the Photon avalanche (PA) process. In particular, the PA process starts at ESA, when ion 2 moves from E1 to the higher

energy state E2. PA upconversion requires an excitation intensity threshold, above which the generation of upconversion luminescence occurs. Below this threshold, minimal upconversion luminescence is observed. In contrast, an increase in upconversion luminescence intensity occurs when the excitation intensity exceeds this threshold. Ion 2 experiences a non-resonant ground-state absorption (GSA) that populates its energy level E1. It is important to remember that the pump wavelength only resonates between the higher energy level E2 and the metastable state E1. Next, using the ESA procedure, ion 2 is excited from the E1 level to the emitting energy level (E2). Two ions (ion 1 and ion 2) are formed in the E1 state as a result of an active CR process between ions 1 and 2. In other words, using this circular mechanism, two ions in the E1 state can function as sensitizer ions to create four more ions, which in turn will create eight more ions. If this pattern is maintained, the population at the E1 level rises (avalanche effect), which



causes the E2 UC emission. Consequently, the PA process has a threshold intensity limit and is time-consuming.<sup>74</sup>

The UCL property of UCNPs could be affected by their different features, for instance the size of these NPs could impacts their luminescence efficiency, so that upconversion emission efficiency diminishing at the nanoscale. This effect is pronounced for UCNPs under 10 nm, where efficiency often falls below 1%.<sup>75,76</sup> They may experience non-radiative deactivation due to interactions with the surrounding medium, surface defects, or ligands, owing to their considerably higher surface-to-volume ratio compared to bulk materials.<sup>77</sup>

The low conversion efficiency of conventional UCNPs, particularly when subjected to low-intensity laser excitation, is a significant drawback. This is mostly because sensitizer  $\text{Yb}^{3+}$  ions absorb light at very low wavelengths in the near-infrared. Therefore, improving NIR light absorption and optimizing the excitation light wavelength into a reasonable range are required to make UCNPs more suited for biological applications.<sup>78</sup> The easiest way to change the excitation wavelength is to use a material that can both absorb and promote the photon upconversion process at the desired wavelength. To address this, incorporating UCNPs with components that strongly absorb around 800 nm is essential. The strong absorption cross-section of  $\text{Nd}^{3+}$  at approximately 800 nm and the effective energy transfer from excited  $\text{Nd}^{3+}$  to  $\text{Yb}^{3+}$  ions make  $\text{Nd}^{3+}$  ions a very promising candidate as the sensitizer to realize the UCL of UCNPs. Accordingly, the excitation wavelength of UCNPs could have blue-shifted with the help of the careful design of the core@shell nanostructure.<sup>78</sup>

The upconversion quantum yield of lanthanide ions is significantly influenced by the composition and structure of the crystal host matrix. Changes in the local crystal field and phonon energy within the matrix affect both radiative and non-radiative transitions, and so play a critical role in determining the overall upconversion efficiency. It is crucial to minimize the phonon energy inside the matrix in order to avoid phonon suppression of UC emission.<sup>77</sup> The crystal structure of the host material impacts the optical properties of the nanocrystals as well. For instance, the hexagonal phase of  $\text{NaYF}_4:\text{Yb}/\text{Er}$  showed better upconversion performs than its variant in the cubic phase.<sup>79</sup> This efficiency difference is related to the crystal-field environment created by the host material's symmetry, which affects the behavior of the trivalent lanthanide ions. Within PTT, the application of excited UPCNs with a wavelength of around 800 nm is noticeable due to its ability to deeply penetrate tissue and serve as an excitation source for different photothermal agents. This is especially important in cases where  $\text{Nd}^{3+}$  sensitized UCNPs that shown strong *in vivo* tumor suppression *via* photothermal effects when paired with Au nanoclusters or  $\text{CuS}$ .<sup>80</sup>

The concentration of dopants in the nanoscale matrix has a major impact on the ability of materials to absorb energy and their upconversion efficiency.<sup>81</sup> Dopant levels need to be carefully managed to limit cross-relaxation events that have the potential to deactivate the higher energy states of the activator ions. To maximize upconversion efficiency,  $\text{Yb}^{3+}$  is typically doped at concentrations between 20% and 30%, depending on

the host matrix and desired emission properties. Activator ions such as  $\text{Er}^{3+}$  or  $\text{Tm}^{3+}$  are usually incorporated at lower concentrations (around 1–2%) to minimize cross-relaxation and concentration quenching.<sup>82</sup> For example,  $\text{Tm}^{3+}$  levels are kept below 1% while  $\text{Er}^{3+}$  dopant levels are typically maintained between 1–3%.<sup>83</sup> This proportion of dopants reduces energy migration between sensitizers ( $\text{Yb}^{3+}-\text{Yb}^{3+}$ ) and substantially assures the isolation between two activating atoms and a piece of  $\text{Yb}^{3+}$ . This enhances the possibility of transferring energy during the upconversion (ETU) process.<sup>84</sup>

The distance between UCNPs and plasmonic structures can influence their upconversion (UC) emission, either enhancing or reducing it depending on the interaction conditions.<sup>85,86</sup> The UC efficiency of UCNPs located near plasmonic structures is influenced by the oscillation of plasmonic electrons in three distinct ways: first, by increasing the absorption of lanthanide ions ( $\text{Ln}^{3+}$ ) through the enhanced intensity of incoming light; second, by increasing the emission intensity through a higher radiative rate of  $\text{Ln}^{3+}$  ions; and third, by decreasing the emission as a result of enhanced non-radiative decay processes. This effect is caused by the plasmon's electron oscillation.<sup>87</sup> To achieve effective PTT, plasmonic NPs like Au or Ag are frequently combined with UCNPs that results in high extinction coefficient and surface plasmonic resonance (SPR) absorption.<sup>88</sup> Besides, UCNPs were used in combination with other types of nanomaterials for PTT applications. Numerous carbon-based materials, including graphene, graphene oxide, carbon nanotubes, graphene dots, and graphene nitride, were successfully used as agents and conjugated with UCNPs for PTT due to their low toxicity and high PT stability.<sup>89</sup> In another research, hollow structures containing lanthanide ions and photothermal agents were developed using  $\text{GdOF}:\text{Ln}$  nanocomposites covered with a silica coating for use in chemotherapy and PTT.<sup>90</sup> Continuing with the development of innovative materials for PTT, researchers have investigated chalcogenide semiconductors such as  $\text{Cu}_x\text{S}$ . They used  $\text{Cu}_x\text{S}$  as a photothermal agent in two-layered hollow spheres made of  $\text{Y}_2\text{O}_3:\text{Yb},\text{Er}/\text{mSiO}_2-\text{Cu}_x\text{S}$ . This combination has demonstrated enhanced effectiveness in PTT and chemotherapy for cancer treatment.<sup>91,92</sup> Additional tests with DOX-loaded  $\text{LaF}_3:\text{Yb}^{3+}/\text{Er}^{3+}/\text{Tm}^{3+}/\text{Nd}^{3+}$  hollow mesoporous spheres demonstrated that NIR laser irradiation significantly improved release efficiency of DOX. Results suggested that  $\text{LaF}_3:\text{Yb}^{3+}/\text{Er}^{3+}/\text{Tm}^{3+}/\text{Nd}^{3+}$  hollow mesoporous spheres could be an excellent choice for multifunctional materials, particularly for PTT due to their enhanced optical heating effect and improved drug release efficiency under NIR laser irradiation.<sup>93</sup> The enhanced photothermal conversion and upconversion emission were observed in  $\text{NaGdF}_4:\text{Yb}^{3+}/\text{Er}^{3+}/\text{Nd}^{3+}/\text{Yb}^{3+}$  and  $\text{NaGdF}_4:\text{Yb}^{3+}/\text{Er}^{3+}/\text{Nd}^{3+}/\text{Yb}^{3+}$  core/shell NPs that were attributed to their spatial separation from the emission core and heating shell, which was in contrast to the NPs that contained only the core. In the case of  $\text{NaGdF}_4:\text{Yb}^{3+}/\text{Er}^{3+}/\text{Nd}^{3+}/\text{Yb}^{3+}$  core/shell NPs, the optical heating and upconversion luminescence were further dependent to the concentration of  $\text{Nd}^{3+}$  in the shell layer. For these  $\text{Er}/\text{Yb}/\text{Yb}/0.7\text{Nd}$  core/shell  $\text{NaGdF}_4$  NPs, the temperature increased up to approximately 10.3 °C when exposed to 808 nm laser light.<sup>94</sup>



Therefore, UCNPs hold great potential for PTT due to their unique ability to convert low-energy NIR light into the higher-energy visible or UV emissions. Their multifunctionality, ranging from deep-tissue imaging and targeted heat generation to photoactivation of therapeutic agents, makes them superior to traditional photothermal materials. The efficiency of UCNPs depends on several factors, including the choice of host matrix, doping ions, particle size, and upconversion mechanisms like ESA, ETU, CSU, CR, and PA. Recent advancements, such as using  $\text{Nd}^{3+}$  ions for 808 nm excitation and designing optimized core@shell structures, have significantly improved their performance while minimizing tissue damage. These advances position UCNPs as powerful tools in next-generation theranostic platforms, particularly for precise and image-guided cancer treatment. In the following section, some of the current researches done on the application of UCNPs for PTT are mentioned in detail.

### 3 Applications of UCNPs in photothermal therapy

#### 3.1 Cancer treatment and targeted therapy

PTT is a localized treatment that has proven to be highly effective in tumor treatment and targeted therapy.<sup>95</sup> This treatment method relies on the generation of heat to damage the targeted cells, and its effectiveness depends on the amount of localized heating produced when exposed to NIR light. Accurate temperature monitoring and control during PTT are essential, as they help minimize damage to surrounding healthy tissues and enhance the precision of the treatment.<sup>96</sup> The optimal temperature range for effectively eliminating tumors is typically in the range of between 42 °C and 45 °C. Maintaining this range is crucial, as it ensures sufficient heat to damage or kill cancer cells without causing excessive harm to surrounding healthy tissue.<sup>97</sup> Temperatures that are too low may result in incomplete tumor destruction, whereas high temperatures can cause damage to surrounding healthy tissues. Therefore, precise temperature control is essential for maximizing the efficacy of PTT. UCNPs are a promising tool for enhancing the precision and efficacy of PTT, particularly in the context of tumor-targeted therapy. These NPs have the potential to improve targeted treatment and localization of the photothermal effect. The integration of UCNPs into PTT offers significant potential for advancing the field of targeted therapy, offering new possibilities for precise and effective treatment of tumors.<sup>98</sup>

The rapid heating of targeted tissue in PTT plays a critical role in reducing damage to the normal cells.<sup>99</sup> Reaching the desired therapeutic temperature in a shorter time minimizes heat diffusion, thereby reducing the risk of damaging surrounding healthy tissues. Application of UCNPs could provide the rapid heating of targeted tissue in PTT. For instance, Liu *et al.* developed a hydrogel complex composed of AuNPs, UCNPs, and alginate hydrogel (UCNPs-Au-Alg) that demonstrated rapid heat generation upon exposure to the 808 nm laser (Fig. 4A), leading to the complete elimination of subcutaneous solid tumors. Under the 808 nm irradiation for 3

minutes, the complex was able to rapidly increase the temperature to 84 °C ( $\Delta T = 52.9$  °C) (Fig. 4B) through the activation of AuNPs by the visible light emitted from the UCNPs. This increasing in the temperature was directly related to the concentration of UCNPs and was specifically achieved locally at the tumor site (Fig. 4C). *In vitro* test showed significant reduction in proliferation of cancer cells in the case of hydrogel exposed with 808 nm laser for 3 minutes (Fig. 4D). Furthermore, tumor growth was inhibited after the initial laser treatment and completely eradicated following a second laser irradiation in a mouse model (Fig. 4E).<sup>99</sup> As could be seen, in here, high level of energy was produced *via* using low-energy light with that has the ability of penetrating into deep part of the body as well. Thus, this formulation could be used for treating cancers in the deep part.

Chu *et al.*, fabricated an UCNPs ( $\text{NaYF}_4\text{:Yb/Er/Nd@NaYF}_4\text{:Nd}$ )@AgBiS<sub>2</sub> core-shell NPs with rapid heating capability under 808 nm laser irradiation, so that utilizing 100  $\mu\text{g mL}^{-1}$  of the nanostructure led to increasing temperature from 25 °C to 56.5 °C after 3 minutes. In contrast, in control group experienced only about 2.3 °C increase in temperature was seen. The findings of this study revealed that the photothermal conversion efficiency of AgBiS<sub>2</sub> was significantly increased from 14.7 to 45% when combined with UCNPs. *In vitro* experiments demonstrated no cytotoxicity effect against normal cell line even at the concentration of 160  $\mu\text{g mL}^{-1}$ , while no cancer cells survived when both of core-shell nanocomposite and NIR irradiation were used. The *in vivo* thermal behavior of this core-shell structure in tumor-bearing mice was investigated and the results indicated that under 808 nm laser irradiation (0.5 W  $\text{cm}^{-2}$ , 10 min), the temperature of the tumor regions rapidly increased to 56.3 °C, while the temperature of tumor in the control group was not obviously change. This substantial temperature elevation effectively suppressed the proliferation of tumor so that no tumor was observed after two weeks of treatment. It was while utilizing NIR or NPs alone couldn't show significant results. Importantly, the treatment had no systemic toxicity, as evidenced by stable body weight in tumor-bearing mice. These results emphasize the potential of UCNPs@AgBiS<sub>2</sub> core-shell NPs for targeted and controlled PTT applications.<sup>100</sup>

UCNPs exhibit responsive luminescence, rendering them valuable as non-contact temperature sensors. Their luminescence intensity and emission wavelength demonstrate sensitivity to temperature fluctuations. Consequently, integrating UCNPs with PTT facilities real-time temperature monitoring during the treatment process and enhances targeting precision and control in cancer therapy.<sup>101</sup> In a study conducted by Zhu *et al.* (2016),<sup>96</sup> the temperature-dependent luminescence properties of UCNPs were utilized for real-time monitoring of temperature during PTT. The research aimed to explore the differences between macroscopic and microscopic temperatures and to assess the effectiveness of PTT at low macroscopic temperatures for tumor ablation. To address this, a carbon-coated core shell upconversion nanocomposite ( $\text{NaLuF}_4\text{:Yb,Er@NaLuF}_4\text{:Carbon}$ ) was synthesized to precisely detect microscopic temperatures. The findings of the study revealed



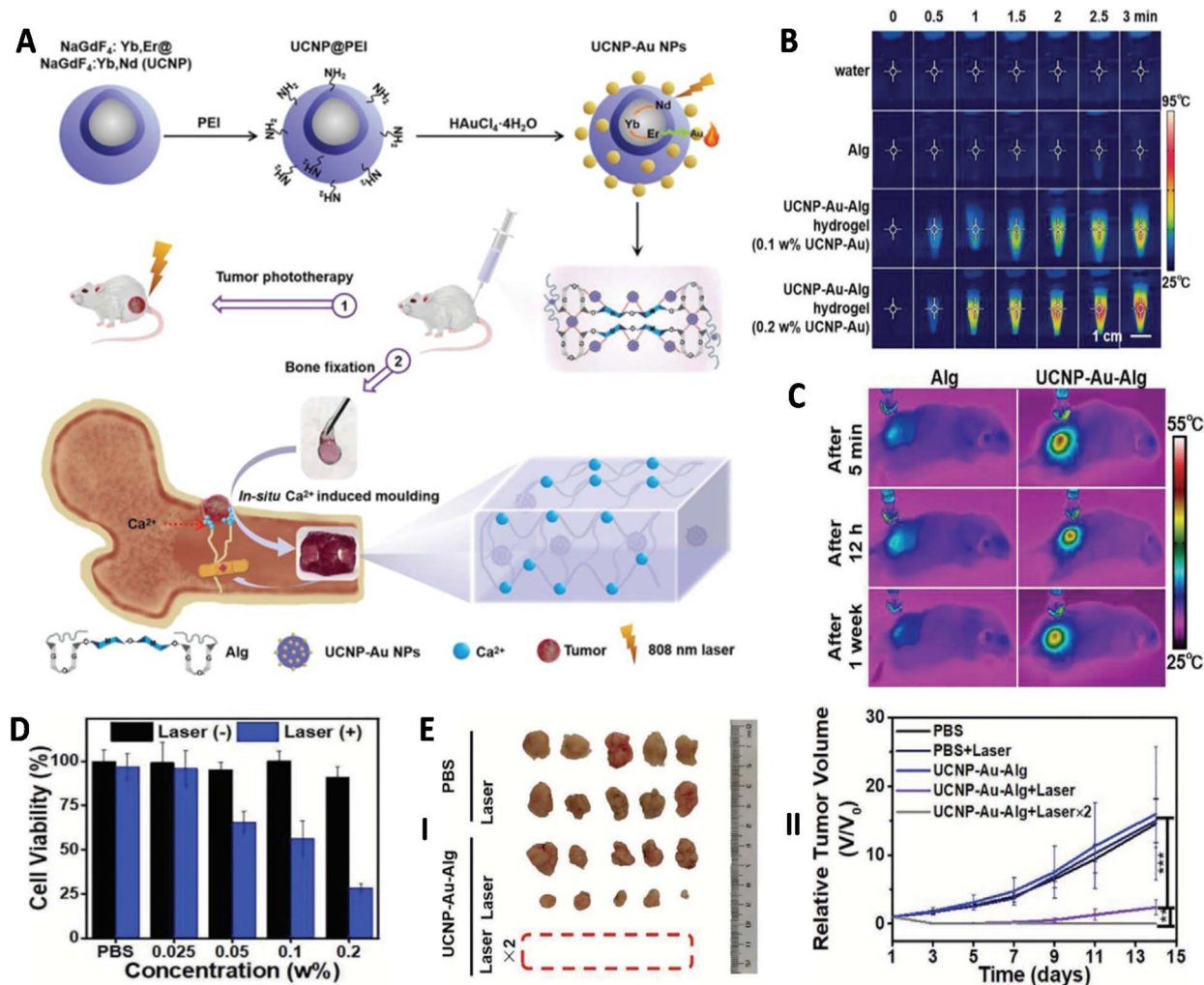


Fig. 4 (A) Schematic image of synthesis and application of UCNPs-Au-Alg hydrogel. (B) Thermal behavior of different materials exposed with 808 nm laser with 1 W cm<sup>-2</sup> for 3 min. (C) Infrared thermal images of the 808 nm laser irradiated mice after injection. (D) Results of cell viability assessment of cancer cells treated with UCNPs-Au-Alg hydrogel in the presence and absence of laser irradiation. (E) Effect of different treatment on size (I) and volume (II) of tumors during 14 days. Reprinted with permission from ref. 99. Copyright 2021, Wiley.

a significant variance between the apparent and microscopic temperatures when exposed to the same irradiation.<sup>96</sup> Via better understanding the temperature dynamics at both macroscopic and microscopic levels, it may be possible to optimize the therapeutic outcomes while minimizing potential adverse effects.

The integration of UCNPs and PTT offers promising opportunities for precise and targeted drug delivery. This synergistic approach employs stimuli-responsive nanocarriers that release therapeutic agents in response to specific triggers such as light, heat, or changes in the tumor microenvironment. UCNPs play a critical role in this system by enabling real-time temperature monitoring to maintain optimal drug release conditions. Moreover, their ability to emit UV light upon NIR excitation allows them to break chemical bonds between drugs and their carriers, thereby facilitating on-demand, localized release and enhancing the overall precision and efficacy of the treatment.<sup>102</sup> This innovative integration allows for remote drug triggering

through thermo-responsive nanocarriers that release drugs at specific temperatures. The photothermal effect converts light to heat, and by incorporating UCNPs, it becomes possible to monitor and achieve the desired temperature for drug release using a non-contact approach. A novel temperature-responsive upconversion core-shell nanostructure was designed in a study for cancer therapy (Fig. 5). This nanostructure demonstrated temperature-dependent luminescence when excited with a 980 nm laser, allowing for precise monitoring of microscopic temperature changes. Moreover, a thermal responsive compound (1,2-dipalmitoyl-*sn*-glycero-3-phosphocholine) was employed for controlled drug delivery. Under NIR excitation at 730 nm, the nanostructure exhibited both photothermal effects and triggered drug release. The core of the nanostructure comprised UCNPs that emitted luminescence, while the surrounding mesoporous silica shell was loaded with the photothermal agent, octabutoxyphthalocyanine palladium(II) (PdPc), and the chemotherapeutic drug doxorubicin. Upon



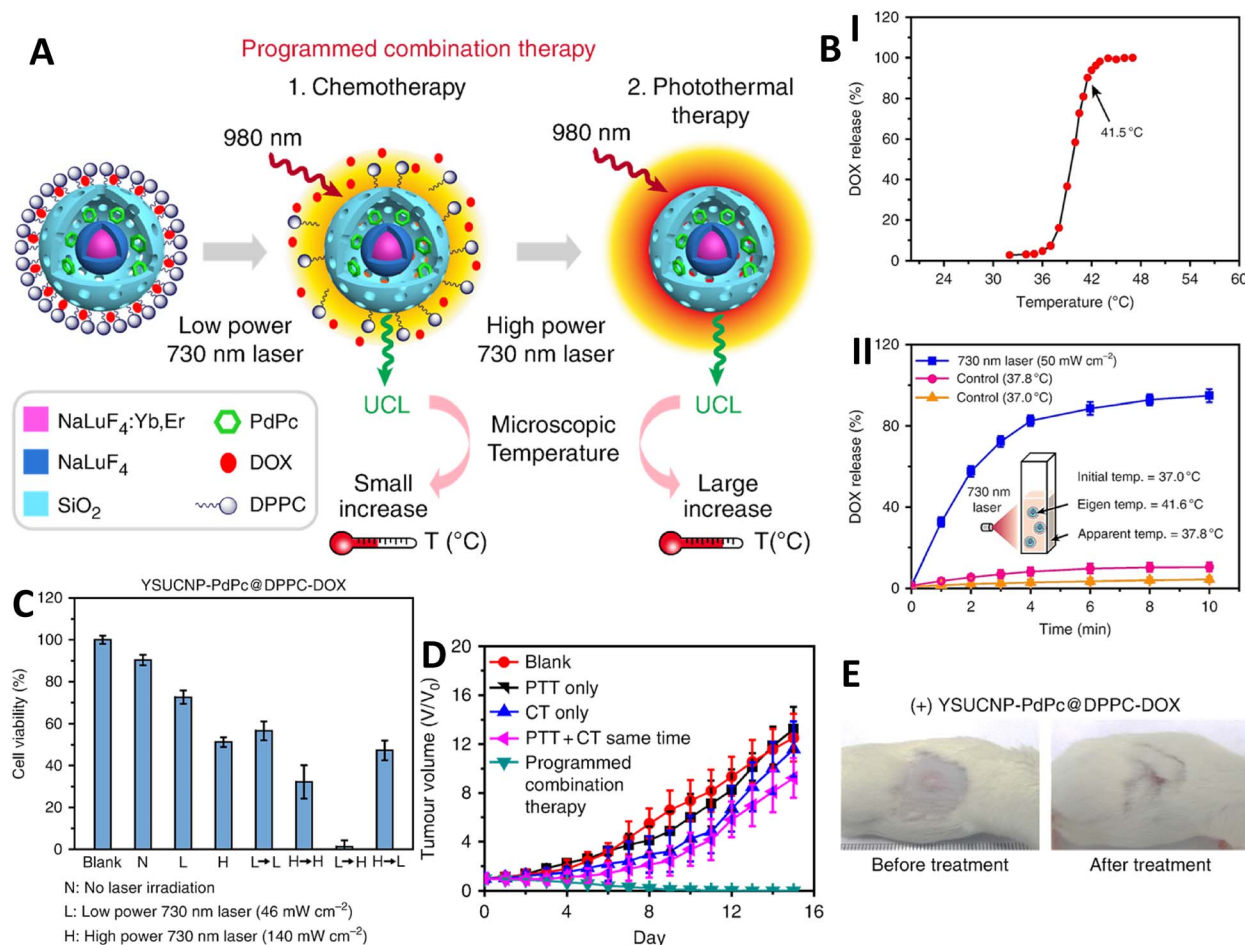


Fig. 5 (A) A schematic diagram illustrating the programmed combination therapy. (B) The release behavior of doxorubicin from the nanosystem under external heating (I), the release rate of doxorubicin from the thermo-responsive nanocomposite over time upon 730 nm laser irradiation (II). (C) Photothermal cytotoxicity based on the viability of cancer cells incubated with YSUCNP-PdPc@DPPC-DOX. (D) Tumor growth in different groups of mice following treatment. (E) Representative images of tumor-bearing mice with programmed combination therapy. Reprinted from ref. 103 under the terms of the Creative Commons CC BY license. Copyright 2018, Nature Inc.

exposure to 730 nm laser irradiation, the temperature of the core-shell nanostructure increased to 41.5 °C, thereby triggering controlled drug release. *In vitro* experiments showed a remarkable improvement in therapeutic effect compared to no laser irradiation group. Furthermore, *in vivo* results confirmed the high efficacy of this therapeutic approach, with complete tumor inhibition observed in tumor-bearing mice.<sup>103</sup>

$\beta$ -NaYF<sub>4</sub>:Yb,Tm UCNP were functionalized with two different types of conjugated polymers, PPVBT-COOH and PDTPT-COOH, which exhibited ideal photodynamic and photothermal features, respectively. Indeed, irradiation of NPs with NIR laser (980 and 808 nm) led to produce UV and visible light by the upconversion part which were adsorbed by the conjugated polymers and led to producing reactive oxygen species (ROS) and increasing temperature by them. The fabricated system showed photothermal stability for a long-time period of application, as well as concentration dependent PD and PT effects, so that the best PD activity was seen at 1 : 1 ratio of conjugated polymers, and the highest increase in temperature was related to the 1 : 2 ratio of PPVBT-COOH to PDTPT.

Therefore, 1 : 1 ratio was selected as the best, and applied against cancer cells. Results of *in vitro* cytotoxicity assay showed no significant toxicity against cancer cells in the absence of light, while irradiating NPs with both of 808 nm and 980 nm laser led to exhibiting significant cytotoxicity (about 90%) at the concentration of 50  $\mu$ g mL<sup>-1</sup>. Results of *in vivo* tests showed fast increasing in the temperature of cancer tissue after 5 min exposing with both 808 nm and 980 nm laser to about 59.3 °C, that was higher than utilizing one laser light. Utilizing both of laser irradiation led to completely remove of tumor, that was while utilizing single laser couldn't completely remove tumor.<sup>104</sup>

### 3.2 Imaging-guided therapy using UCNP

UCNPs are highly versatile and promising tools in the field of biomedical imaging that offer several advantages over traditional imaging agents. Their strong resistance to photobleaching and photoblinking makes them highly suitable for prolonged bioimaging applications. Additionally, their ability to emit visible or UV upon excitation by NIR light allows for deeper tissue penetration and reduced background autofluorescence,





resulting in clearer and more accurate imaging. Additionally, their low toxicity and high biocompatibility make them ideal for *in vivo* imaging applications. One of the key factors contributing to their versatility is their ability to be doped with various imaging agents. This characteristic enables UCNPs to be used in multimodal imaging approaches, which can utilize the strengths of different imaging modalities.<sup>105,106</sup> For instance, a matrix of  $K_{0.3}Bi_{0.7}F_{2.4}$  UCNP was synthesized with excellent upconversion luminescence under 980 nm laser irradiation. The strong upconversion luminescence emitted by  $K_{0.3}Bi_{0.7}F_{2.4}:Yb^{3+}/Tm^{3+}$  NPs make them suitable for deep tissue optical imaging. The fabricated NPs showed high signal-to-noise ratio at the tumor site and good biocompatibility in *in vivo* test.<sup>107</sup> Choi *et al.*, developed a multi-shell structured UCNP composed of  $NaYF_4:Yb/Er$  core covered with three different shells contained  $Tm^{3+}/Nd^{3+}$  that was then functionalized with Rose Bengal and Chlorin e6 (as photosensitizers (PSs)) and folic acid (FA) (as targeting agent). Presence of FA led to enhancing cellular uptake of NPs by the cancer cells that overexpressed FA receptor so that much higher fluorescence intensity was observed by these cells. Exposing NPs with 808 nm laser led to the production of ROS so that the amounts of ROS in the case of NPs with both PSs was higher compared to each PS alone. Results of cell viability test showed that cells exposed with different concentrations of NPs had no toxicity effect at dark conditions, while utilizing laser irradiation led to a significant reduction in viability of cancer cells. Results of cytotoxicity test showed concentration and intensity dependent cytotoxicity effect so that higher toxicity was observed by increasing the concentration of NPs and intensity of laser.<sup>108</sup>

A switchable core-shell NP was fabricated *via* covering the  $NaYF_4:Yb, Er$  (the core part) with mesoporous polydopamine (mPDA) (as shell) functionalized with L-Arg and indocyanine green (ICG), which were used as nitric oxide (NO) generator and phototherapeutic compound, respectively. It was a theranostic compound that exhibited upconversion luminescence after irradiated with 980 nm laser light, that was switch to therapy format after exposing with 808 nm light. In here, ICG acted as both photosensitizer and photothermal compound that produced ROS and increased the temperature of its surrounded environment after exposing with 808 nm light. It could also aid L-Arg in producing NO gas through acting as an oxidant molecule. The fabricated formulation showed dose and time dependent photothermal performance so that utilizing concentration of about  $400 \mu g mL^{-1}$  and 10 min irradiation led to increasing the temperature to about  $52.8^\circ C$ . Results of *in vitro* tests showed no significant cytotoxicity effect in the absence of light, while irradiating cells with NIR laser led to the toxicity effect.<sup>109</sup>

Ye *et al.* proposed a multifunctional targeted nanoplatform for simultaneous diagnosis and treatment of cancer cells. It was composed of  $NaYF_4:Yb, Er$  UCNPs covered with polydopamine (PDA) and functionalized with ICG and FA attached to the poly(ethylene glycol) (PEG). The presence of ICG in the structure of this system enhanced its PDT and PTT properties. FA, on the other hand, provided the targeting ability of the formulation and PEG enhanced circulation time of the fabricated NP.

Presence of UCNP provided the capability of imaging from the cells contained NPs irradiated with 980 nm NIR light. Besides, irradiating cells with 808 nm laser led to a rapid increase in the temperature to about  $60^\circ C$ , that confirmed PTT effect of the NPs related to the presence of both ICG and UCNP. Besides, ICG induced the production of ROSs inside cells in a time dependent manner. Moreover, the loaded ICG showed much higher amounts of ROSs compared to the free ICG. The combination of these two method led to a significant anticancer activity after just 10 min NIR irradiation.<sup>110</sup> Therefore, the combination uses of UCNPs and ICG could introduce an ideal candidate for diagnosis and treatment of cancer. It has been found that X-ray f-lanthanide ions (*e.g.*,  $Lu^{3+}$ ,  $Yb^{3+}$ ) possess significant potential for X-ray attenuation and can effectively function as Computed Tomography (CT) contrast agents.<sup>111</sup>

In another study, the development of a nanohybrid core-multi-shell ( $NaYF_4:Yb, Er@NaLuF_4:Yb@NaNdF_4:Yb@NaLuF_4:Yb-Bi_2Se_3$ ) was developed, enabling the integration of bimodal imaging and efficient photothermal conversion. The presence of Lanthanide (Lu, Yb) and Bi elements in this nanohybrid enabled reasonable computed tomography (CT) imaging capabilities, while efficient luminescence was provided by  $Lu^{3+}$ -based UCNPs. Under 808 nm near-infrared laser irradiation, the UCNPs emitted visible light, and the  $Bi_2Se_3$  nanomaterial efficiently converted light into heat. The UCNP- $Bi_2Se_3$  nanohybrid demonstrated satisfactory therapeutic efficacy *in vitro*. Under 808 nm irradiation, almost no viable cancer cells were observed due to the photothermal effect. Additionally, when cells incubated with UCNPs and exposed to 980 nm laser power, green luminescence emission was detected. The Hounsfield Unit (HU) value demonstrated a concentration-dependent increase, and cells incubated with the nanohybrid exhibited enhanced and distinguishable CT contrast. Overall, this nanohybrid exhibited effective cancer cell killing, strong upconversion luminescence, and clear CT contrast, highlighting its potential as a promising theragnostic agent for non-invasive dual imaging-guided PTT.<sup>112</sup>

In addition to photoluminescent imaging, it is possible to incorporate imaging contrast for other modalities such as magnetic resonance imaging (MRI) and positron emission tomography (PET) into UCNPs. By doping different elements into the UCNP structure, it becomes possible to integrate multimodality imaging capabilities with PTT functionalities within a single platform.<sup>111</sup> For instance, Zhang *et al.* have developed a multifunctional nanocomposite using UCNPs and black phosphorous nanosheets (BPNs) for multimodal imaging and therapy. This nanocomposite, composed of UCNPs from the  $NaYF_4:Yb/Er/Nd$  type exhibited PTT, PDT, and multimodal imaging (MR, fluorescence, optoacoustic, ultrasonic imaging) for efficient cancer treatment and diagnosis. The UCNPs converted low-energy light to high-energy type, which was then absorbed by black phosphorous and Chlorin e6 (Ce6) for PTT and PDT as well as a fluorescent imaging agent.  $MnO_2$  was used for the conversion of  $H_2O_2$  to the  $O_2$  in tumor microenvironment, which was essential for Ce6 and BPNs mediated PDT therapy. Doping  $Fe_3O_4$  and  $MnO_2$  NPs provided T1 and T2 MRI contrast, respectively. Under 808 nm laser irradiation, the



temperature of physiologic solution was increased with increasing nanocomposite concentration, resulting in a photo-thermal conversion efficiency of about 33.4%. *In vitro* experiments showed sufficient generation of ROS by the nanocomposite that confirmed its potential application for PDT. Cellular uptake investigations revealed that the nanocomposite could enter to the cytoplasm but not the cell nuclei. When treating cancer cells with the nanocomposite under NIR irradiation, cell viability was significantly reduced, while no cytotoxicity results were obtained at dark condition. The nanocomposite demonstrated effective PTT, with tumor temperatures exceeding 50 °C within five minutes of 808 nm

laser irradiation in tumor-bearing mice, resulting in significant tumor growth inhibition. Importantly, the nanocomposite induced no systemic adverse effects on mice body weight, and all mice receiving both the nanocomposite and irradiation survived (100% survival). The T1 and T2 longitudinal relaxivity of nanocomposite had linear relationship with the concentration of  $\text{Mn}^{2+}$  and  $\text{Fe}_3\text{O}_4$ , respectively. Additionally, when Ce6 was doped into the nanocomposite, it exhibited a high photoluminescence intensity, albeit lower than free Ce6.<sup>113</sup>

A hybrid core-shell NP of  $\text{NaDyF}_4\text{:Lu@Prussian Blue}$  was fabricated in a study for multifunctional imaging-guided PTT (Fig. 6). This nanocomposite demonstrated the ability to

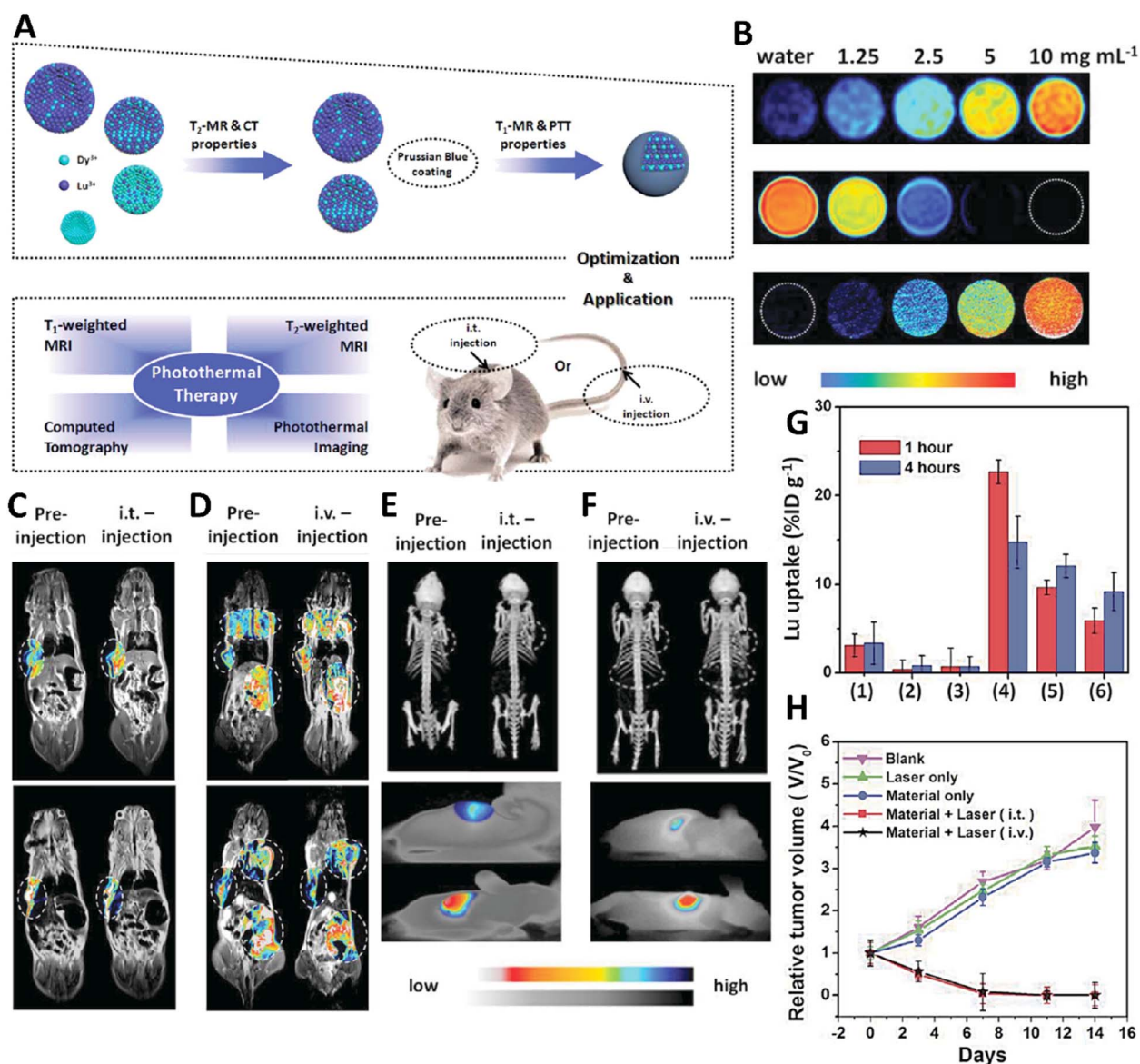


Fig. 6 (A) Scheme of fabricating, optimizing, and applying  $\text{NaDyF}_4\text{:Lu@Prussian blue}$  used for multifunctional imaging-guided PTT. (B) Color-map related to the  $\text{T}_1$  (top) and  $\text{T}_2$  weighted MR and CT (bottom) images of different concentrations of  $\text{NaDyF}_4\text{:Lu@PB}$ . Multimodal imaging capability of fabricated  $\text{NaDyF}_4\text{:Lu@Prussian blue}$  nanomaterial:  $\text{T}_1$ - (C) and  $\text{T}_2$ -weighted MRI (D), CT scan (E), and photothermal (F). (G) The amounts of  $\text{NaDyF}_4\text{:Lu@Prussian blue}$  presented in tumor and vital organs of mice after 1 and 4 h of injecting  $\text{NaDyF}_4\text{:Lu@Prussian blue}$  ((1) lung, (2) kidney, (3) heart, (4) liver, (5) spleen, and (6) tumor.) (H) Effect of different treatment on tumor volume during 14 days. Reprinted with permission from ref. 114. Copyright 2016, Wiley.



generate both T1 and T2-weighted MRI contrast, attributed to the presence of  $\text{Dy}^{3+}$  and  $\text{Lu}^{3+}$  ions and Prussian blue, as well as CT signal from the  $\text{Dy}^{3+}$  and  $\text{Lu}^{3+}$ . Additionally, Prussian Blue served as the PTT agent. The nanocomposite exhibited an enhanced contrast signal in T1- and T2-weighted MRI. Furthermore, it achieved enhanced contrast signals in CT imaging compared to water. The multifunctional nanocomposite demonstrated a high CT value of 253 HU at the concentration of  $10 \text{ mg mL}^{-1}$ . Notably, the nanocomposites effectively accumulated in tumors within an hour, indicating passive tumor targeting. Injection of the nanocomposite at the tumor site led to enhanced contrast in both MR and CT imaging, facilitating improved tumor visualization. Photothermal imaging demonstrated increasing in thermal signal at the tumor site, reaching to about  $45^\circ\text{C}$  within 5 min. *In vivo* experiments demonstrated that the relative tumor volume decreased to zero, indicating that the nanocomposite, upon NIR light irradiation, served as a highly effective modality for photothermal cancer therapy. Overall, the fabricated nanocomposite held promise as a MRI, CT imaging and PTT agent.<sup>114</sup>

Ni *et al.* synthesized a theranostic nanoplatfrom that integrated PTT, radiotherapy (RT), and multimodal MRI/CT/UCL imaging. The nanoplatfrom consisted of CuS NPs (as the photothermal agent) wrapped around UCNPs with a manganese dioxide ( $\text{MnO}_2$ ) coating. The UCNPs, composed of  $\text{NaGdF}_4\text{:Yb,Er@NaGdF}_4\text{:Yb,Nd}$ , provided luminescence imaging and enhanced photothermal conversion. The  $\text{MnO}_2$  coating acted as a T1 contrast agent for MRI, while the inherent properties of the UCNPs, due to the presence of  $\text{Yb}^{3+}$ , provided T2 contrast enhancement. There was a linear relationship between MR signal intensity and the concentration of nanocomposite. The nanocomposite demonstrated strong CT imaging capability, with CT values increasing proportionally with its concentration, indicating excellent contrast-enhancing properties. Additionally,  $\text{MnO}_2$  interacted with  $\text{H}_2\text{O}_2$  in the tumor microenvironment, leading to abundant oxygen generation and reducing hypoxia. This enhancement in oxygen availability contributed to the improved RT outcomes. The nanoplatfrom demonstrated biocompatibility and successful internalization by HepG2 cells. Photothermal conversion efficiency of the nanoplatfrom showed increasing the temperature to about  $40^\circ\text{C}$  under the 1064 nm laser irradiation. Furthermore, in a combination radiation and photothermal treatment, most of the cells were destroyed. *In vivo* fluorescent imaging revealed the accumulation of the nanocomposite at the tumor site. Notably, in mice treated with the nanocomposite under NIR irradiation and radiotherapy, tumor volume was significantly suppressed. Importantly, this nanoplatfrom showed no systemic adverse effect and all mice treated with the combinational RT/PTT remain in good health.<sup>115</sup>

A core-shell nanoplatfrom consisting of  $\text{Ag}_2\text{Se}$  nanodots on the surface of chitosan coated UCNP (UCNPs@CS@ $\text{Ag}_2\text{Se}$ ) was developed for multimodal imaging-guided PTT (Fig. 7). This multifunctional nanoplatfrom integrated various imaging modalities (UCL, DSL, CT, and photoacoustic (PA)) with PTT for cancer theranostic. The UCNP ( $\text{NaYF}_4\text{:Yb/Er@NaLuF}_4\text{:Nd/Yb@NaLuF}_4$ ) was acted as upconversion luminescence imaging

(UCL) compound and downshifting luminescence (DLS) agent that converted low-energy light to the high energy one, while the  $\text{Ag}_2\text{Se}$  nanodots efficiently absorbed NIR light and converted it to heat, leading to localized hyperthermia. Lutetium ions ( $\text{Lu}^{3+}$ ) and ytterbium ions ( $\text{Yb}^{3+}$ ) were applied as CT imaging compounds. The chitosan coating improved biocompatibility and stability of nanoplatfrom. In this study, the signal intensity of PA, CT and UCL exhibited a linear increase with rising nanocomposite concentrations. It was a biocompatible nanocomposite that exhibited a photothermal conversion efficiency of about 37.6% and was capable of raising the temperature above  $50^\circ\text{C}$  in aqueous solution under 808 nm laser irradiation. Notably, Under NIR-laser irradiation, tumor size was significantly decreased in tumor-bearing mice injected with the nanocomposite. Furthermore, after the injection of the nanocomposite, the signal intensity gradually increased in all types of imaging within 2 h. This gradual increase indicated homogeneous accumulation of nanocomposite at the tumor site. Subsequently, the intensity decreased by 24 h, likely due to the metabolism of a portion of the nanocomposite. Taken together, the fabricated UCNPs-based nanocomposite showed great promise as a multifunctional theranostic agent.<sup>116</sup>

### 3.3 UCNPs in tissue engineering and regenerative medicine

The integration of UCNPs and PTT in tissue engineering shows great potential. UCNPs can convert NIR light to higher energy light, making them valuable for non-invasive tissue engineering. PTT offers diverse applications within tissue engineering field, including antibacterial effects, promotion of angiogenesis and cell growth, tumor ablation, and targeted drug delivery. However, PTT have limitations that UCNPs can address to enhance their applicability in tissue engineering. Different applications require specific temperature ranges: mild local heat ( $41\text{--}43^\circ\text{C}$ ) stimulates cell proliferation and angiogenesis, while moderate heat ( $45\text{--}50^\circ\text{C}$ ) can selectively damage tumor cells and hyperthermia ( $>50^\circ\text{C}$ ) can inhibit bacterial proliferation but risks harming healthy tissue. Therefore, precise temperature control is crucial. UCNPs, with their temperature-dependent luminescence, can aid in monitoring tissue temperature during PTT, ensuring safety and optimal therapeutic outcomes.<sup>117,118</sup>

The development of NIR-upconversion hydrogels (NIRUH) has brought about several advantages, including the ability to penetrate deep tissues safely and trigger hydrogel precursors' photopolymerization. Additionally, NIRUH possesses antibiofilm features by emitting UV light. A modified NIRUH (NIR mediated orthogonal upconversion photochemistry (NIRUPP)), was fabricated by Liu *et al.*, to address the challenges of low NIR upconversion efficiency and photochemical efficiency, and moderate mechanical properties (Fig. 8). The NIRUCH precursor was consisted of ruthenium complex ( $\text{Ru}(\text{bpy})_3^{2+}$ ), persulfate salt, UCNPs ( $\text{NaYbF}_4\text{:Gd}^{3+}/\text{Tm}^{3+}\text{@NaGdF}_4\text{:Nd}^{3+}/\text{Yb}^{3+}\text{@NaGdF}_4\text{:Nd}^{3+}/\text{Yb}^{3+}$ ), gelatin, and polymerizable monomers. Under 808 nm NIR irradiation, UCNPs emitted 450 nm fluorescence which was absorbed by  $\text{Ru}(\text{bpy})_3^{2+}$ , leading to the generation of radical sulfate and initiating the polymerization



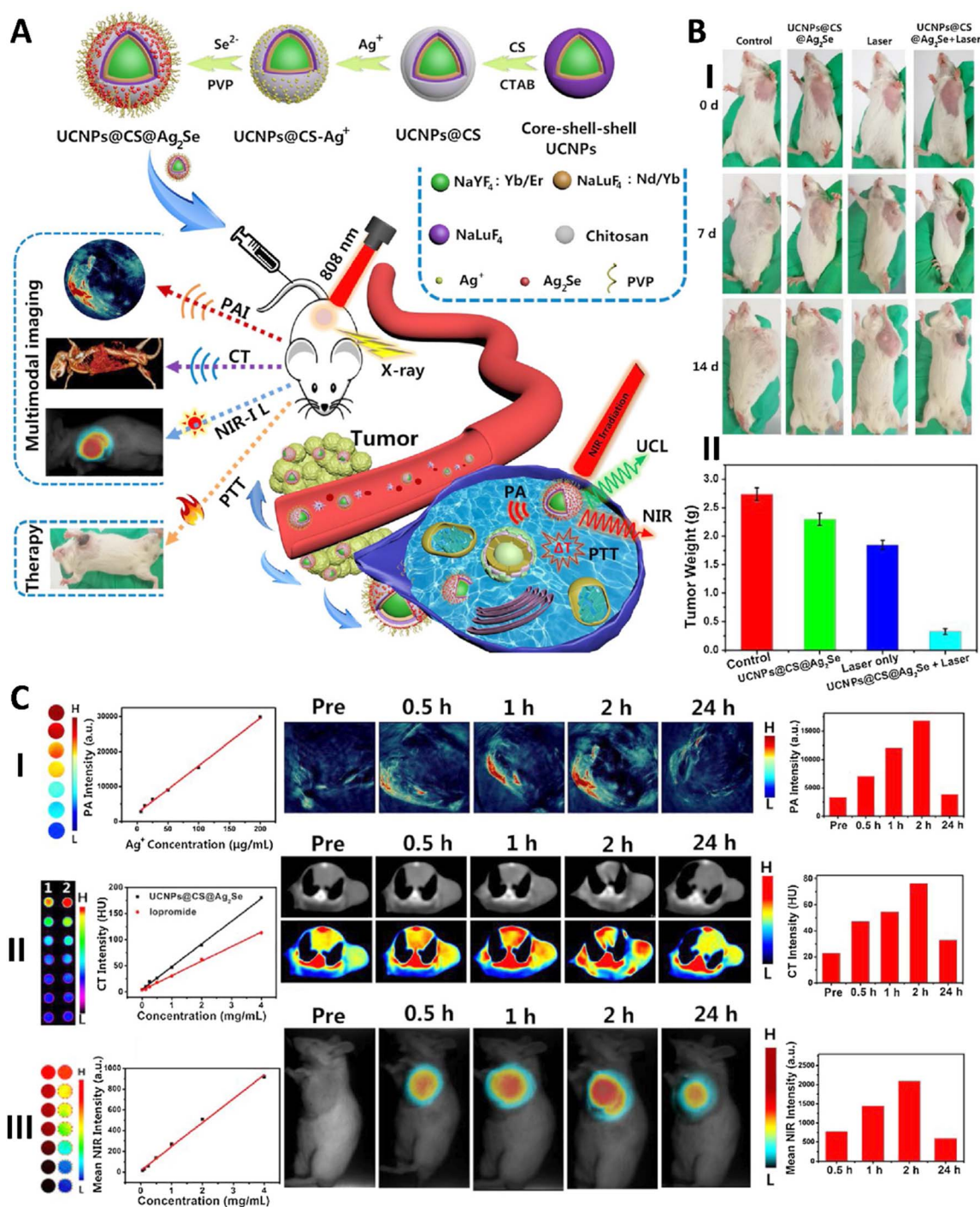


Fig. 7 (A) Schematic image related to the fabrication and application of UCNPs@CS@Ag<sub>2</sub>Se nanocomposites for multifunctional imaging-guided PTT. (B) Representative photographs of mice on different groups after various treatments (I), mean tumor weight of each group after various treatments from the last day of the experiment (II). (C) *In vitro* and *in vivo*, PA images (I), CT images (II), NIR images (III). Reprinted with permission from ref. 116. Copyright 2019, Elsevier Inc.

of vinyl monomers, resulting in the formation of a gel network. The UCNPs were interfacially engineered with oleic acid, improving their interactions with the gel matrix and minimizing unwanted energy transfer to water in the surrounding medium. Additionally, upconvert fluorescence quenching was minimized, allowing efficient energy transfer to the Ru(bpy)<sub>3</sub><sup>2+</sup>

complexes. The enhanced fluorescence acted as an initiator for gel formation, enabling the rapid fabrication of underlying tissue structures within just 45 to 240 seconds. Mechanical parameters of NIROUP were also improved by UCNPs so that the critical strain, maximum stress, and toughness reach to 10 kPa, 275 kPa and 900 kJ m<sup>-3</sup>, respectively (2, 3.5 and 6 times higher





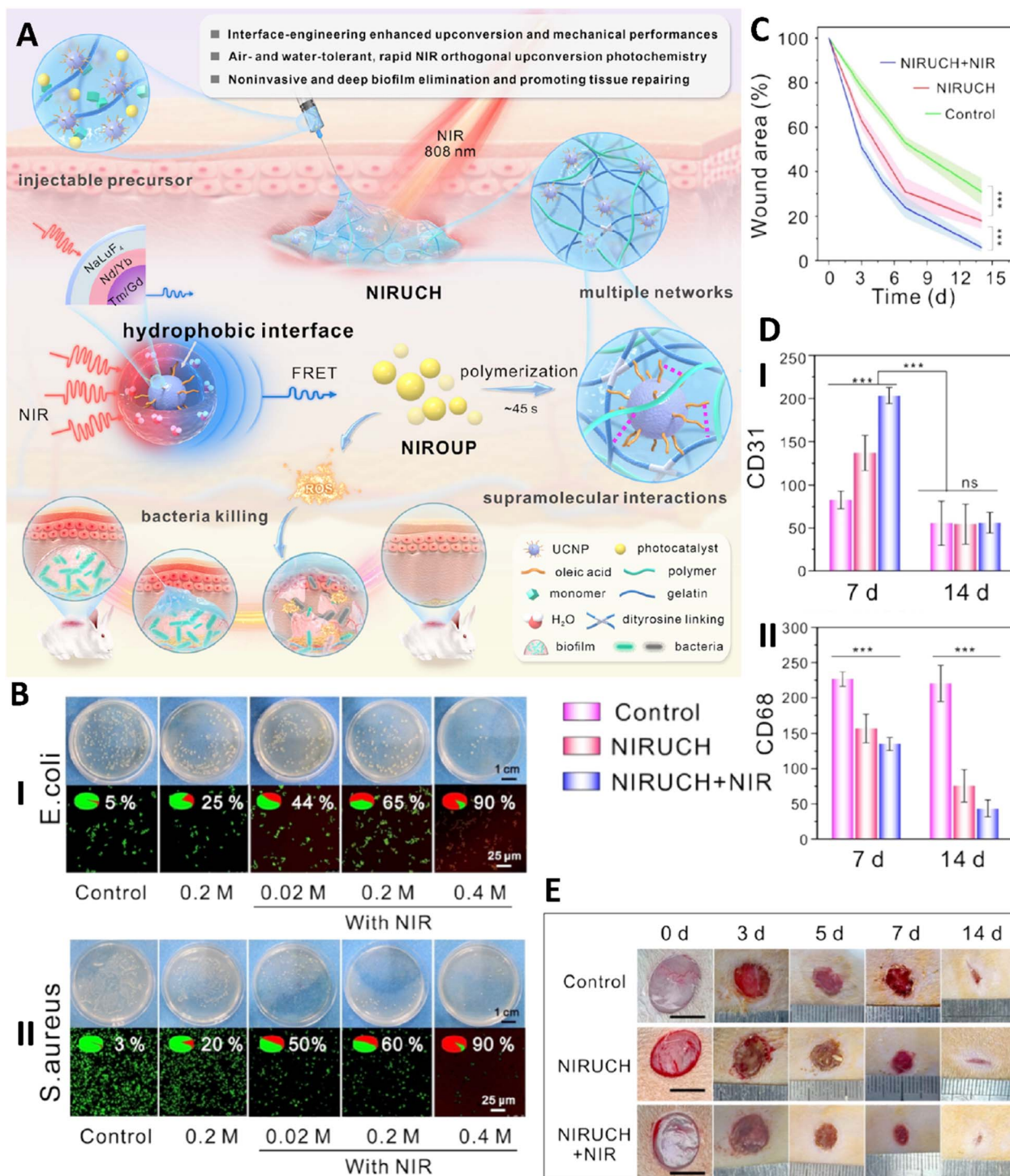


Fig. 8 (A) Schematic image of fabrication of UCNP-based hydrogel (NIRUCH) and its application as antibacterial wound healing compound. (B) Antibacterial activity of NIRUCH in the presence/absence of NIR irradiation against *E. coli* (I) and *S. aureus* (II). (C) Effect of NIRUCH (with/without NIR irradiation) on wound area. (D) Anti-inflammatory effect of NIRUCH (with/without NIR irradiation) during 14 days. (E) Image of wound healing process during 14 days for different samples. Reprinted with permission from.<sup>119</sup> Copyright 2024, ACS.

than those in single-network hydrogels). Furthermore, the NIRUCH exhibited ~75% elasticity recovery within just 2 min and near complete recovery within 5 min. *In vitro* results showed that the hydrogel inhibited the growth of Gram-positive and Gram-negative bacteria nearly 100% under NIR irradiation by

releasing hydroxyl radical. *In vivo* experiments also revealed antibiofilm properties so that effectively killed *Staphylococcus aureus* (*S. aureus*) through hydroxyl radical generation under NIR irradiation. Moreover, the hydrogels exhibited excellent wound healing ability, with wound closure rates exceeding 95%



after 14 days. More importantly, this strategy demonstrated the capability for tissue repair underneath due to the deep penetration of NIR irradiation. 21 days after injecting the precursor into wounds beneath rabbit skin, the wounds were almost fully healed. Taken together, the fabricated modified-NIRUH offered rapid gel formation, impressive mechanical properties, wound healing capabilities, and biofilm resistance under NIR irradiation. The ability to trigger gel formation remotely *via* NIR made them compatible with remote printing technology.<sup>119</sup>

UCNPs, in combination with photoactivatable ligands, enable precise control over biological processes. By utilizing NIR light, researchers can activate these ligands on demand, guiding cells to attach and form new blood vessels in a controlled manner within a 4D hydrogel environment. Zheng *et al.* developed a NIR-reactive hydrogel by integrating UCNPs and hydrogels to control the differentiation of endothelial cells and trigger angiogenesis in 3D culture. UCNPs (NaYF<sub>4</sub>:TmYb) were embedded in PEG thiol/(maleic anhydride alt-1-octadecene) hydrogel (UCNP-PMAO) containing a UV-triggerable cell-adhesive peptide (cyclo(RGD(DMNPB)FC)). Under 974 nm laser irradiation, the emitted UV light from UCNPs activated the peptide as a model photoactivatable molecule. Besides, under NIR irradiation, L929 cells spread within the hydrogel, resulting in an increased aspect ratio, while in the absence of NIR, cells remained spherical and did not spread. Furthermore, Human umbilical vein endothelial cells (HUVECs) embedded in the hydrogel exhibited angiogenesis under NIR, forming an interconnected microvascular network after 24 h of laser irradiation. But, in the absence of NIR light, cells maintained the rounded morphology and didn't form microvascular network. Therefore, UCNPs embedded in photoresponsive hydrogels could hold promise for use in 4D tissue engineering and regenerative medicine applications.<sup>120</sup>

Non-invasive monitoring of tissue-engineered implants in the body is a challenge in the field of medical research. One potential solution is the use of UCNPs as a photoluminescence agent within the scaffold. In a study conducted by M. Trifanova *et al.*, UCNPs were incorporated into scaffolds to impart photoluminescence properties. In this investigation, both natural and synthetic polymer were loaded with NaYF<sub>4</sub>:Yb<sup>3+</sup>, Er<sup>3+</sup>/NaYF<sub>4</sub> nanocrystals without any surface modification. Notably, scaffolds exhibited no cytotoxic effect on Bj-5ta fibroblasts. The polymeric scaffold was subcutaneously implanted in female BALB/c mice, resulting in an intensity of photoluminescence that monotonically decreased with time due to the gradual degradation of the scaffolds within the animal tissue. Histological analysis of the implantation zone revealed a moderate inflammatory response in the tissue surrounding the implanted scaffolds. Based on these results, the UCNPs-assisted luminescent bioimaging enabled continuous monitoring of the scaffold.<sup>121</sup>

## 4 Challenges

The photothermal applications of UCNPs present a set of challenges that need to be addressed to optimize their effectiveness in various biomedical fields. One of the key challenges

is maximizing the photothermal conversion efficiency of UCNPs, ensuring that they can efficiently convert NIR light into heat for targeted therapy. Achieving uniform heating across the target tissue area while minimizing damage to surrounding healthy cells is crucial for successful PTT. Additionally, challenges related to the stability and biocompatibility of UCNPs need to be carefully considered to prevent potential toxicity or adverse effects in biological systems. The design of UCNPs, including their size, shape, surface modifications, and targeting ligands, plays a critical role in overcoming these challenges and enhancing their performance in photothermal applications. Furthermore, issues such as optimal dosing, biodistribution, and clearance of UCNPs from the body are important factors that require thorough investigation to ensure their safe and effective use in clinical settings.<sup>3,122–124</sup>

Biocompatibility considerations are integral to the successful integration of UCNPs and PTT in various biomedical applications.<sup>125</sup> Challenges related to biocompatibility involve various factors that must be carefully addressed to guarantee the safety and effectiveness of UCNPs in clinical settings. One key challenge is the potential cytotoxicity of UCNPs, which can arise from factors such as particle size, surface charge, and composition. Understanding the interactions of UCNPs with biological systems and their impact on cellular function is essential for evaluating their biocompatibility. Additionally, immune responses triggered by UCNPs must be carefully studied to assess any inflammatory reactions or immune cell activation.<sup>126</sup> The long-term effects of UCNPs within the body, including their biodistribution, accumulation, and potential toxicity over time, are also critical considerations that need to be thoroughly investigated. To address these challenges, researchers are exploring novel surface modifications, biodegradable coatings, and bioconjugation strategies to enhance the biocompatibility of UCNPs while preserving their photothermal properties. Additional explorations ought to be focused on advancing biocompatibility testing methods, conducting in-depth studies on the biological fate of UCNPs, and developing standardized protocols for evaluating the safety of UCNPs in biomedical applications. By overcoming these challenges and prioritizing biocompatibility considerations, the integration of UCNPs and PTT holds significant promise for revolutionizing personalized medicine, regenerative therapies, and targeted cancer treatments with enhanced safety and efficacy.

Tumor targeting strategies are vital in improving the efficacy and specificity of photothermal applications using UCNPs in cancer therapy.<sup>4,10</sup> Several methods have been devised to target tumors selectively and deliver UCNPs to the tumor microenvironment, maximizing the photothermal effect on cancer cells while minimizing damage to healthy tissues. One common strategy involves functionalizing UCNPs with targeting ligands, such as antibodies or peptides, that can recognize and bind to specific receptors overexpressed on cancer cells. This targeted approach enables UCNPs to accumulate preferentially in tumor tissues, enhancing the precision of PTT. Additionally, passive targeting mechanisms exploit the EPR effect of tumors, enabling UCNPs to accumulate in tumor tissues owing to their leaky vasculature and compromised lymphatic drainage.



Combining active and passive targeting strategies can further enhance the specificity and effectiveness of UCNP in tumor targeting. Challenges in tumor targeting include optimizing the design of targeting ligands for efficient tumor recognition, improving UCNP's circulation time and stability in the bloodstream, and overcoming biological barriers to reach deep-seated tumors. Future directions in tumor targeting strategies using UCNP may involve the development of multifunctional nanosystems that combine targeting moieties with imaging capabilities, drug delivery functionalities, and theranostic properties to enable personalized and precise cancer treatments. By advancing tumor targeting strategies, researchers aim to develop cancer therapy by leveraging the unique capabilities of UCNP for targeted photothermal applications, ultimately improving patient outcomes and minimizing side effects associated with traditional cancer treatments.<sup>105,106</sup>

One of the significant challenges in the application of UCNP in PTT is the limitations posed by NIR light penetration in biological tissues.<sup>10</sup> NIR light is commonly used to excite UCNP and induce photothermal effects; however, its penetration depth is limited by tissue absorption and scattering properties. As a result, deep-seated tumors or tissues located beyond the reach of NIR light may not receive sufficient light energy to activate UCNP effectively. This shallow penetration depth of NIR light poses a challenge in achieving uniform heating and therapeutic efficacy in deeper tissues, potentially compromising the success of PTT using UCNP. Researchers are exploring various strategies to overcome this limitation, such as optimizing the wavelength of light used for excitation, developing advanced light delivery systems, and incorporating imaging techniques to guide light delivery to target tissues more accurately. Additionally, efforts are being made to enhance the tissue-penetrating capabilities of UCNP by improving their photothermal conversion efficiency and exploring alternative light sources with deeper tissue penetration, such as photoacoustic or multiphoton excitation methods. By addressing the limitations of NIR light penetration in biological tissues, researchers aim to improve the depth of tissue treatment and expand the applicability of UCNP in PTT for a broader range of clinical scenarios.<sup>1,125</sup> Future advancements in this area may lead to innovative solutions that enhance the therapeutic outcomes and effectiveness of UCNP in cancer treatment and tissue engineering applications.

Optimizing the photothermal conversion efficiency of UCNP is crucial for maximizing their efficacy in photothermal applications, including cancer therapy and tissue engineering.<sup>127</sup> The photothermal conversion efficiency refers to the ability of UCNP to efficiently convert absorbed light energy into heat, which is essential for inducing localized hyperthermia in targeted tissues. Several strategies can be employed to enhance the photothermal conversion efficiency of UCNP, including optimizing their composition, size, and surface properties. By carefully selecting the materials used in UCNP and tuning their structural characteristics, researchers can improve the absorption of light at specific wavelengths and enhance the conversion of light energy into heat. Surface modifications, including plasmonic coatings or functional groups, can significantly

enhance photothermal conversion efficiency of UCNP by enhancing their light absorption and thermal stability. Furthermore, controlling the aggregation state of UCNP and minimizing energy loss mechanisms, such as non-radiative decay processes, can further boost their photothermal performance. Future research directions may focus on developing novel nanomaterials, exploring advanced light-matter interactions, and optimizing the design of UCNP to achieve higher photothermal conversion efficiencies for more effective and targeted photothermal therapies.<sup>1,2</sup> By enhancing the photothermal conversion efficiency of UCNP, researchers strive to enhance treatment outcomes, shorten treatment durations, and reduce side effects linked to conventional cancer therapies, ultimately advancing the field of nanomedicine and personalized healthcare.

The clinical translation of UCNP for biomedical applications requires careful consideration of regulatory requirements, safety profiles, and scalability for widespread clinical use.<sup>125,128</sup> As UCNP move towards clinical trials and potential commercialization, regulatory agencies play a critical role in evaluating their safety, efficacy, and quality standards to ensure patient safety and treatment effectiveness. Addressing regulatory considerations involves conducting comprehensive preclinical studies, optimizing manufacturing processes, and obtaining regulatory approvals for clinical testing. Furthermore, collaborations between researchers, clinicians, industry partners, and regulatory agencies are essential to facilitate the successful translation of UCNP from the laboratory to clinical practice. By navigating regulatory challenges, establishing safety guidelines, and meeting quality standards, the clinical translation of UCNP holds the potential to revolutionize healthcare practices, improve patient results, and shape the future of nanomedicine as a vital component of modern medicine.

Future research directions will focus on addressing these challenges through advanced NP design, innovative imaging techniques, and comprehensive biocompatibility studies to unlock the full potential of UCNP in PTT and other biomedical applications. By overcoming these challenges, researchers aim to harness the unique properties of UCNP for precise and targeted photothermal treatments, ultimately improving patient results in several medical scenarios.

## 5 Future prospects

The future prospects of photothermal applications using UCNP hold tremendous promise for advancing precision medicine, cancer therapy, and tissue engineering. By harnessing the unique photothermal properties of UCNP, researchers aim to develop innovative strategies for targeted hyperthermia, localized therapy, and theranostic applications. Future advancements in this field may focus on optimizing the design of UCNP for enhanced photothermal conversion efficiency, improving light delivery systems for deeper tissue penetration, and exploring new approaches for combining PTT with other treatment modalities. Additionally, advancements in imaging-guided therapy using UCNP for real-time monitoring of treatment responses and personalized treatment regimens are



expected to drive the development of more effective and tailored therapeutic approaches. The integration of UCNPs in combination therapies, multifunctional nanosystems, and regenerative medicine applications holds the potential to transform healthcare practices by providing precise, targeted, and minimally invasive treatment options.

The future prospects of UCNPs in biomedical applications involve the development of multifunctional UCNPs that can offer enhanced therapeutic outcomes. By integrating multiple functionalities into UCNPs, such as imaging, drug delivery, and PTT capabilities, researchers aim to create versatile nanoplatforms that can address various aspects of disease diagnosis and treatment simultaneously. Multifunctional UCNPs have the potential to develop personalized medicine by enabling customized and precise treatment strategies based on individual patient characteristics. These advanced nanosystems may open new avenues for targeted therapy, theranostics, and regenerative medicine applications, offering innovative solutions for complex healthcare challenges.

Combination therapies involving UCNPs represent a promising approach to enhance the efficacy of cancer treatments and overcome drug resistance. By integrating UCNPs with other therapeutic approaches, such as chemotherapy, immunotherapy, or gene therapy, researchers can develop synergistic treatment regimens that target multiple pathways involved in tumorigenesis. These combination therapies have the potential to improve treatment outcomes, reduce side effects, and prevent disease recurrence by harnessing the distinct properties of UCNPs for targeted drug delivery and localized therapy. Future research efforts will focus on optimizing combination therapy protocols, identifying synergistic treatment modalities, and translating these innovative approaches into clinical practice for improved patient care.

Advancements in NP engineering are essential for unlocking the full potential of UCNPs in biomedical applications. By refining the design, synthesis, and characterization of UCNPs, researchers can enhance their physicochemical properties, biocompatibility, and therapeutic efficacy. Innovative NP engineering strategies, such as controlled drug release mechanisms, stimuli-responsive coatings, and bioconjugation techniques, offer new opportunities to tailor the behavior of UCNPs for specific biomedical applications. Future advancements in NP engineering will concentrate on creating next-generation UCNPs with improved stability, targeting capabilities, and therapeutic functionalities, setting the stage for advanced nanomedicine solutions and personalized healthcare interventions.

## 6 Conclusion

UCNPs have attracted considerable attention in recent years because of their distinctive optical properties. These NPs have the ability to convert low-energy photons into higher-energy photons through a process called upconversion. This property makes UCNPs highly suitable for a variety of photothermal applications. However, there are several challenges that need to be addressed to further optimize and advance this technique. One of the key challenges in the use of UCNPs for PTT is

ensuring their biocompatibility. While UCNPs have shown low toxicity in many studies, it is crucial to conduct thorough investigations to evaluate their long-term effects on the body. Grasping the interactions between UCNPs and biological systems is crucial to minimize any potential side effects and maximize their therapeutic benefits. Strategies need to be developed to enhance the accumulation of UCNPs specifically in tumor tissues while minimizing their uptake by healthy tissues. Improving the selectivity and specificity of UCNPs for tumor cells will greatly enhance the effectiveness of PTT and reduce off-target effects. Although UCNPs have the advantage of converting low-energy NIR light into higher-energy visible light, the penetration depth of NIR light in tissues is limited. This restricts the application of PTT to superficial tumors or requires invasive procedures for deep tissue targeting. Overcoming this challenge will involve developing innovative strategies to enhance NIR light penetration and delivery to the target site. In addition, the photothermal conversion efficiency of UCNPs is another important factor to consider. Higher conversion efficiency would allow for lower light doses to achieve the desired therapeutic effect, reducing the risk of damaging healthy tissues. Enhancing the photothermal conversion efficiency of UCNPs through material design and optimization is an ongoing area of research. Future developments in UCNPs for PTT will focus on designing multifunctional NPs that combine PTT with other therapeutic modalities or imaging techniques. By incorporating drug delivery systems or imaging agents onto UCNPs, synergistic effects can be achieved, leading to more effective and personalized cancer treatments. Combining PTT with other treatment modalities, such as chemotherapy or immunotherapy, offers significant potential for improving cancer treatment outcomes. UCNPs can be utilized to transfer therapeutic agents to the tumor site, amplifying the synergistic effects of combination therapies and overcoming drug resistance. Advancements in NP engineering will further enhance the properties and functionalities of UCNPs. Tailoring the size, shape, and surface chemistry of UCNPs can optimize their photothermal conversion efficiency, biocompatibility, and tumor-targeting capabilities. Moving forward, efforts should be focused on the translation of UCNPs for PTT from the laboratory to clinical settings. Extensive preclinical studies, toxicity evaluations, and optimization of synthesis and scale-up methods are necessary steps towards clinical trials. The purpose of this review is to analyze and assess the current state of research, highlight the potential benefits and challenges of utilizing these NPs in PTT, and provide valuable insights for further advancements and applications in the field.

## Data availability

No data was used for the research described in the article.

## Author contributions

Masoomah Amoozadeh: writing – review & editing; Danial Khorsandi: writing – review & editing; Amin Farahani: writing – review & editing; Atefeh Zarepour: writing – review & editing;



Arezoo Khosravi: visualization, writing – review & editing; Siavash Iravani: supervision, conceptualization, writing – review & editing; Ali Zarrabi: supervision, writing – review & editing.

## Conflicts of interest

The authors declare no conflict of interests.

## Acknowledgements

Ali Zarrabi acknowledges funding support from the 2535 – International Bilateral Cooperation Funding Program of The Scientific and Technological Research Council of Türkiye (TÜBİTAK, Project No. 121N152).

## References

- H. E. Gültekin, G. Yaşayan, A. Bal-Öztürk, A. Bigham, A. Simchi, A. Zarepour, S. Iravani and A. Zarrabi, *Mater. Horiz.*, 2024, **11**, 363–387.
- R. S. Ajee, P. S. Roy, S. Dey and S. Sundaresan, *J. Nanopart. Res.*, 2024, **26**, 50.
- R. Rafique, S. K. Kailasa and T. J. Park, *TrAC, Trends Anal. Chem.*, 2019, **120**, 115646.
- R. Wang, H. Yang, R. Fu, Y. Su, X. Lin, X. Jin, W. Du, X. Shan and G. Huang, *Cancers*, 2020, **12**, 3136.
- X. Cui, Q. Ruan, X. Zhuo, X. Xia, J. Hu, R. Fu, Y. Li, J. Wang and H. Xu, *Chem. Rev.*, 2023, **123**, 6891–6952.
- X. Yu, S. Fan, B. Zhu, S. I. El-Hout, J. Zhang and C. Chen, *Green Energy Environ.*, 2024, DOI: [10.1016/j.gee.2024.09.002](https://doi.org/10.1016/j.gee.2024.09.002).
- X. Li, F. Zhang and D. Zhao, *Chem. Soc. Rev.*, 2015, **44**, 1346–1378.
- G. Liang, H. Wang, H. Shi, H. Wang, M. Zhu, A. Jing, J. Li and G. Li, *J. Nanobiotechnol.*, 2020, **18**, 154.
- A. A. Ansari, A. K. Parchur, N. D. Thorat and G. Chen, *Coord. Chem. Rev.*, 2021, **440**, 213971.
- M. K. Mahata, R. De and K. T. Lee, *Biomedicines*, 2021, **9**, 756.
- P. Dash, P. K. Panda, C. Su, Y.-C. Lin, R. Sakthivel, S.-L. Chen and R.-J. Chung, *J. Mater. Chem. B*, 2024, **12**, 3881–3907.
- S. Borse, R. Rafique, Z. V. P. Murthy, T. J. Park and S. K. Kailasa, *Analyst*, 2022, **147**, 3155–3179.
- Y. Lin, Y. Yao, W. Zhang, Q. Fang, L. Zhang, Y. Zhang and Y. Xu, *Acta Biomater.*, 2021, **135**, 1–12.
- G. Xiang, Q. Xia, X. Liu, Y. Wang, S. Jiang, L. Li, X. Zhou, L. Ma, X. Wang and J. Zhang, *Nanoscale*, 2021, **13**, 7161–7168.
- M. Ovais, S. Mukherjee, A. Pramanik, D. Das, A. Mukherjee, A. Raza and C. hen, *Adv. Mater.*, 2020, **32**, 2000055.
- X. Zhu, W. Feng, J. Chang, Y.-W. Tan, J. Li, M. Chen, Y. Sun and F. Li, *Nat. Commun.*, 2016, **7**, 10437.
- H. Zhao, L. Zhao, Z. Wang, W. Xi, S. T. Dibaba, S. Wang, L. Shi and L. Sun, *J. Mater. Chem. B*, 2019, **7**, 3652–3660.
- E. M. Mettenbrink, W. Yang and S. Wilhelm, *Adv. Photonics Res.*, 2022, **3**, 2200098.
- Y. Li, C. Chen, F. Liu and J. Liu, *Microchim. Acta*, 2022, **189**, 109.
- J. Lee, A. C. Gordon, H. Kim, W. Park, S. Cho, B. Lee, A. C. Larson, E. A. Rozhkova and D.-H. Kim, *Biomaterials*, 2016, **109**, 69–77.
- E. M. Trifanova, M. A. Khvorostina, A. O. Mariyanats, A. V. Sochilina, M. E. Nikolaeva, E. V. Khaydukov, R. A. Akasov and V. K. Popov, *Molecules*, 2022, **27**, 6547.
- M. González-Béjar, L. Francés-Soriano and J. Pérez-Prieto, *Front. Bioeng. Biotechnol.*, 2016, **4**, 47.
- Y. Xing, L. Li, X. Ai and L. Fu, *Int. J. Nanomedicine*, 2016, **11**, 4327–4338.
- S. Han, B. W. Hwang, E. Y. Jeon, D. Jung, G. H. Lee, D. H. Keum, K. S. Kim, S. H. Yun, H. J. Cha and S. K. Hahn, *ACS nano*, 2017, **11**, 9979–9988.
- A. Zumla, *Lancet Infect. Dis.*, 2010, **10**, 303–304.
- R. W. Habash, R. Bansal, D. Krewski and H. T. Alhafid, *Critical Reviews™ in Biomedical Engineering*, 2006, **34**, 491–542.
- S. Guo, D. Gu, Y. Yang, J. Tian and X. Chen, *J. Nanobiotechnol.*, 2023, **21**, 348.
- D. T. Debela, S. G. Muzazu, K. D. Heraro, M. T. Ndalama, B. W. Mesele, D. C. Haile, S. K. Kitui and T. Manyazewal, *SAGE Open Med.*, 2021, **9**, 20503121211034366.
- X. Xu, X. Liu, L. Tan, Z. Cui, X. Yang, S. Zhu, Z. Li, X. Yuan, Y. Zheng and K. W. K. Yeung, *Acta Biomater.*, 2018, **77**, 352–364.
- F. Cortezon-Tamarit, H. Ge, V. Mirabello, M. B. Theobald, D. G. Calatayud and S. Pascu, in *Inorganic and Organometallic Transition Metal Complexes with Biological Molecules and Living Cells*, Elsevier, 2017, pp. 245–327.
- J. R. Melamed, R. S. Edelstein and E. S. Day, *ACS Nano*, 2015, **9**, 6–11.
- S. Areekara, A. Sabu, A. Mathew, K. Parvathy and P. Rana, *J. Therm. Anal. Calorim.*, 2023, **148**, 8945–8968.
- C. Li, Y. Cheng, D. Li, Q. An, W. Zhang, Y. Zhang and Y. Fu, *Int. J. Mol. Sci.*, 2022, **23**, 7909.
- W. Li, J. Peng, L. Tan, J. Wu, K. Shi, Y. Qu, X. Wei and Z. Qian, *Biomaterials*, 2016, **106**, 119–133.
- Y. Yang, W. Zhu, Z. Dong, Y. Chao, L. Xu, M. Chen and Z. Liu, *Adv. Mater.*, 2017, **29**, 1703588.
- X. Deng, W. Guan, X. Qing, W. Yang, Y. Que, L. Tan, H. Liang, Z. Zhang, B. Wang and X. Liu, *ACS Appl. Mater. Interfaces*, 2020, **12**, 4265–4275.
- S. Kumari, N. Sharma and S. V. Sahi, *Pharmaceutics*, 2021, **13**, 1174.
- W. Zeng, Z. Li, H. Chen, X. Zeng and L. Mei, *Cell Rep. Phys. Sci.*, 2022, **3**(6), 100898.
- G. Sanità, B. Carrese and A. Lamberti, *Front. Mol. Biosci.*, 2020, **7**, 587012.
- J. Li, W. Zhang, W. Ji, J. Wang, N. Wang, W. Wu, Q. Wu, X. Hou, W. Hu and L. Li, *J. Mater. Chem. B*, 2021, **9**, 7909–7926.
- Z. Chen, R. K. Kankala, L. Long, S. Xie, A. Chen and L. Zou, *Coord. Chem. Rev.*, 2023, **481**, 215051.
- M. Rizwan Younis, G. He, B. Gurram, J. Lin and P. Huang, *Adv. NanoBiomed Res.*, 2021, **1**, 2100029.





- 43 R. S. Riley and E. S. Day, *Wiley Interdiscip. Rev.: Nanomed. Nanobiotechnol.*, 2017, **9**, e1449.
- 44 A. Shakeri-Zadeh and S. K. Kamrava, in *Biomaterials for Precision Cancer Medicine*, Elsevier, 2025, pp. 93–122.
- 45 Y. Xing, R. Jing, J. Kang, Y. Li, H. Zhang, X. Tang and Z. Jiang, *Curr. Med. Chem.*, 2025, **32**, 238–257.
- 46 N. Guha and M. K. Zaman, in *Nanocarriers Based Colon Targeting*, Elsevier, 2025, pp. 261–284.
- 47 W. Wang, P. Gao, H. Gui, X. Wei, H. Zhang and X. Wang, *Coord. Chem. Rev.*, 2025, **522**, 216205.
- 48 A. Gangwar, S. Gupta, J. Gupta, B. Dutta, N. Dubey, S. B. Shelar, N. Singh, S. Biswas, P. Hassan and K. Barick, *J. Photochem. Photobiol., A*, 2025, **459**, 116084.
- 49 S. Liu, R. Ding, J. Yuan, X. Zhang, X. Deng, Y. Xie and Z. Wang, *ACS Appl. Mater. Interfaces*, 2024, **16**, 3001–3018.
- 50 L. Xu, H. Guo, Y. Zhong, Y.-e. Zhao and L. Lin, *Int. J. Biol. Macromol.*, 2024, **279**, 135479.
- 51 D. Hu, M. Zha, H. Zheng, D. Gao and Z. Sheng, *Research*, 2025, **8**, 0583.
- 52 W. Feng, X. Mu, Y. Li, S. Sun, M. Gao, Y. Lu and X. Zhou, *Acta Biomater.*, 2024, **185**, 371–380.
- 53 J. Zhao, X. Zheng, E. P. Schartner, P. Ionescu, R. Zhang, T. L. Nguyen, D. Jin and H. Ebendorff-Heidepriem, *Adv. Opt. Mater.*, 2016, **4**, 1507–1517.
- 54 Y. Tian, Y. Tian, P. Huang, L. Wang and Q. Shi, *Chem. Eng. J.*, 2016, **297**, 26–34.
- 55 G. Liang, H. Wang, H. Shi, H. Wang, M. Zhu, A. Jing, J. Li and G. Li, *J. Nanobiotechnol.*, 2020, **18**, 1–22.
- 56 E. Hong, L. Liu, L. Bai, C. Xia, L. Gao, L. Zhang and B. Wang, *Mater. Sci. Eng., C*, 2019, **105**, 110097.
- 57 N. Dubey and S. Chandra, *J. Rare Earths*, 2022, **40**, 1343–1359.
- 58 H. S. Naher, B. A. H. Al-Turaihi, S. H. Mohammed, S. M. Naser, M. A. Albark, H. A. Madloul, H. A. M. Al-Marzoog and A. T. Jalil, *J. Drug Delivery Sci. Technol.*, 2023, **80**, 104175.
- 59 H. Zhang, X. Wang, R. Jin and Q. Su, *Giant*, 2022, **12**, 100130.
- 60 Q. Q. Dou, H. C. Guo and E. Ye, *Mater. Sci. Eng., C*, 2014, **45**, 635–643.
- 61 M. Wang, G. Abbineni, A. Clevenger, C. Mao and S. Xu, *Nanomed. Nanotechnol. Biol. Med.*, 2011, **7**, 710–729.
- 62 M. Meng, T. Zhang, J. Wang, Z. Cheng, Y. Liu, X. Qiao, J. Wen, U. Resch-Genger, W. Long and J. Ou, *ACS Appl. Nano Mater.*, 2022, **6**, 759–771.
- 63 S. T. Dibaba, Y. Xie, W. Xi, A. Bednarkiewicz, W. Ren and L. Sun, *J. Rare Earths*, 2022, **40**, 862–869.
- 64 A. J. Kandeloos, S. Bastani, M. Ghahari, M. Jalili and J. Lalevée, *Polym. Eng. Sci.*, 2024, **64**, 4630–4652.
- 65 R. Luo, C. Zhang, Z. Zhang, P. Ren, Z. Xu and Y. Liu, *Nanoscale*, 2025, **17**, 2985–3002.
- 66 M. N. Islam and A. Bag, in *Smart Nanosensors*, Springer, 2025, pp. 301–364.
- 67 S. Geng, H. Li, Z. Lv, Y. Zhai, B. Tian, Y. Luo, Y. Zhou and S. T. Han, *Adv. Mater.*, 2025, 2419678.
- 68 G. Chen, H. Qiu, P. N. Prasad and X. Chen, *Chem. Rev.*, 2014, **114**, 5161–5214.
- 69 K. Lingeswar Reddy, R. Balaji, A. Kumar and V. Krishnan, *Small*, 2018, **14**, 1801304.
- 70 N. Xin, D. Wei, Y. Zhu, M. Yang, S. Ramakrishna, O. Lee, H. Luo and H. Fan, *Mater. Today Chem.*, 2020, **17**, 100329.
- 71 F. Auzel, *Chem. Rev.*, 2004, **104**, 139–174.
- 72 M. Xue, X. Zhu, X. Qiu, Y. Gu, W. Feng and F. Li, *ACS Appl. Mater. Interfaces*, 2016, **8**, 17894–17901.
- 73 G. Xiang, Y. Ma, W. Liu, J. Wang, Z. Gu, Y. Jin, S. Jiang, X. Luo, L. Li and X. Zhou, *Inorg. Chem.*, 2017, **56**, 13955–13961.
- 74 M.-F. Joubert, *Opt. Mater.*, 1999, **11**, 181–203.
- 75 U. Resch-Genger and H. H. Gorris, *Anal. Bioanal. Chem.*, 2017, **409**, 5855–5874.
- 76 C. Würth, S. Fischer, B. Grauel, A. P. Alivisatos and U. Resch-Genger, *J. Am. Chem. Soc.*, 2018, **140**, 4922–4928.
- 77 F. Wang and X. Liu, *Chem. Soc. Rev.*, 2009, **38**, 976–989.
- 78 X. Li, F. Zhang and D. Zhao, *Chem. Soc. Rev.*, 2015, **44**, 1346–1378.
- 79 S. Heer, K. Kömpe, H. U. Güdel and M. Haase, *Adv. Mater.*, 2004, **16**, 2102–2105.
- 80 X. Xie, Z. Li, Y. Zhang, S. Guo, A. I. Pendharkar, M. Lu, L. Huang, W. Huang and G. Han, *Small*, 2017, **13**, 1602843.
- 81 J. Matias, K. Komolibus, W. Kiang, S. Konugolu-Venkata-Sekar and S. Andersson-Engels, *Nanoscale*, 2024, **16**, 3641–3649.
- 82 X. Zhu, J. Zhang, J. Liu and Y. Zhang, *Advanced Science*, 2019, **6**, 1901358.
- 83 F. Souissi, Fabrication and Optical Properties of Upconverting Nanoparticle/ Graphene Hybrids, PhD thesis, Université d'Ottawa/University of Ottawa, 2024.
- 84 M.-J. Monks, C. Würth, E. Kemnitz and U. Resch-Genger, *Nanoscale*, 2022, **14**, 11590–11599.
- 85 J. Kumar and I. Roy, *Talanta Open*, 2024, **9**, 100302.
- 86 M. K. Abraham, A. S. Madanan, S. Varghese, A. I. Shkhaier, G. Indongo, G. Rajeevan, N. Vijila and S. George, *Analyst*, 2024, **149**, 231–243.
- 87 G. Tessitore, G. A. Mandl, M. G. Brik, W. Park and J. A. Capobianco, *Nanoscale*, 2019, **11**, 12015–12029.
- 88 S. Yuan, J. Zhou, J. Wang, X. Ma, F. Liu, S. Chen, J.-X. Fan and G.-P. Yan, *Mol. Pharm.*, 2024, **21**(2), 467–480.
- 89 N. Singh, R. S. Gupta and S. Bose, *Nanoscale*, 2024, **16**, 3243–3268.
- 90 A. A. Ansari, A. K. Parchur and G. Chen, *Coord. Chem. Rev.*, 2022, **457**, 214423.
- 91 B. Lin, J. Liu, Y. Wang, F. Yang, L. Huang and R. Lv, *Chem. Mater.*, 2020, **32**, 4627–4640.
- 92 E. Balciunaite, N. Petrasauskiene, R. Alaburdaite, G. Jakubauskas and E. Paluckiene, *Surf. Interfaces*, 2020, **21**, 100801.
- 93 R. Lv, G. Yang, F. He, Y. Dai, S. Gai and P. Yang, *Nanoscale*, 2014, **6**, 14799–14809.
- 94 Q. Shao, Z. Yang, G. Zhang, Y. Hu, Y. Dong and J. Jiang, *ACS Omega*, 2018, **3**, 188–197.
- 95 N. Gupta and R. Malviya, *BBA, Biochim. Biophys. Acta, Rev. Cancer*, 2021, **1875**, 188532.
- 96 X. Zhu, W. Feng, J. Chang, Y.-W. Tan, J. Li, M. Chen, Y. Sun and F. Li, *Nat. Commun.*, 2016, **7**, 10437.



- 97 X. Zhang, B. Tan, Y. Wu, M. Zhang and J. Liao, *Polymers*, 2021, **13**, 2100.
- 98 H. Chen, B. Ding, P. a. Ma and J. Lin, *Adv. Drug Delivery Rev.*, 2022, **188**, 114414.
- 99 B. Liu, X. Gu, Q. Sun, S. Jiang, J. Sun, K. Liu, F. Wang and Y. Wei, *Adv. Funct. Mater.*, 2021, **31**, 2010779.
- 100 Z. Chu, T. Tian, Z. Tao, J. Yang, B. Chen, H. Chen, W. Wang, P. Yin, X. Xia, H. Wang and H. Qian, *Bioact. Mater.*, 2022, **17**, 71–80.
- 101 A. Sedlmeier, D. E. Achatz, L. H. Fischer, H. H. Gorris and O. S. Wolfbeis, *Nanoscale*, 2012, **4**, 7090–7096.
- 102 G. Lee and Y. I. Park, *Nanomaterials*, 2018, **8**, 511.
- 103 X. Zhu, J. Li, X. Qiu, Y. Liu, W. Feng and F. Li, *Nat. Commun.*, 2018, **9**, 2176.
- 104 X. Guo, L. Li, W. Jia, C. Zhang, W. Ren, C. Liu and Y. Tang, *ACS Appl. Mater. Interfaces*, 2024, **16**, 19926–19936.
- 105 L. Cheng, K. Yang, Y. Li, J. Chen, C. Wang, M. Shao, S. T. Lee and Z. Liu, *Angew. Chem., Int. Ed.*, 2011, **50**, 7385–7390.
- 106 Y. Min, J. Li, F. Liu, P. Padmanabhan, E. K. Yeow and B. Xing, *Nanomaterials*, 2014, **4**, 129–154.
- 107 R. An, P. Lei, P. Zhang, X. Xu, J. Feng and H. Zhang, *Nanoscale*, 2018, **10**, 1394–1402.
- 108 J. Choi and S. Y. Kim, *Appl. Mater. Today*, 2023, **31**, 101755.
- 109 Y. Jiang, Y. Hong, Y.-Y. Liu, Y. Guan, J. Zhou, H. Wang and L. Sun, *J. Mater. Chem. C*, 2024, **12**, 11938–11947.
- 110 S. Ye, W. Zhang, Y. Shen, S. Han, H. Hu, Y. Liang, Z. Lin, Y. Jin, T. Lawson and Y. Liu, *Macromol. Rapid Commun.*, 2023, **44**, 2300298.
- 111 D. Wang, B. Liu, Z. Quan, C. Li, Z. Hou, B. Xing and J. Lin, *J. Mater. Chem. B*, 2017, **5**, 2209–2230.
- 112 S. Zhao, R. Tian, B. Shao, Y. Feng, S. Yuan, L. Dong, L. Zhang, Z. Wang and H. You, *Chem. - Eur. J.*, 2020, **26**, 1127–1135.
- 113 Q. Zhang, W. Wang, M. Zhang, F. Wu, T. Zheng, B. Sheng, Y. Liu, J. Shen, N. Zhou and Y. Sun, *Chem. Eng. J.*, 2020, **391**, 123525.
- 114 Y. Liu, Q. Guo, X. Zhu, W. Feng, L. Wang, L. Ma, G. Zhang, J. Zhou and F. Li, *Adv. Funct. Mater.*, 2016, **26**, 5120–5130.
- 115 J. Ni, H. Xu, Y. Zhong, Y. Zhou and S. Hu, *J. Mater. Chem. B*, 2022, **10**, 549–561.
- 116 K. Du, P. Lei, L. Dong, M. Zhang, X. Gao, S. Yao, J. Feng and H. Zhang, *Appl. Mater. Today*, 2020, **18**, 100497.
- 117 V. Dediu, J. Ghitman, G. Gradisteanu Pircalabioru, K. H. Chan, F. S. Iliescu and C. Iliescu, *Int. J. Mol. Sci.*, 2023, **24**, 9375.
- 118 L. He, D. Di, X. Chu, X. Liu, Z. Wang, J. Lu, S. Wang and Q. Zhao, *J. Controlled Release*, 2023, **363**, 180–200.
- 119 J. Liu, B. Zhang, Z. Lu, J.-W. Shen, P. Zhang and Y. Yu, *Chem. Mater.*, 2024, **36**(12), 6276–6287.
- 120 Y. Zheng, Z. Chen, Q. Jiang, J. Feng, S. Wu and A. Del Campo, *Nanoscale*, 2020, **12**, 13654–13661.
- 121 E. M. Trifanova, G. Babayeva, M. A. Khvorostina, A. V. Atanova, M. E. Nikolaeva, A. V. Sochilina, E. V. Khaydukov and V. K. Popov, *Life*, 2023, **13**, 870.
- 122 W. Feng, C. M. Han and F. Y. Li, *Adv. Mater.*, 2013, **25**, 5287–5303.
- 123 W. Feng, X. Zhu and F. Li, *NPG Asia Mater.*, 2013, **5**, e75.
- 124 J. Ferrera-González, L. Francés-Soriano, C. Galiana-Roselló, J. González-García, M. González-Béjar, E. Fröhlich and J. Pérez-Prieto, *Biomedicines*, 2021, **9**, 1419.
- 125 H. Oliveira, A. Bednarkiewicz, A. Falk, E. Fröhlich, D. Lisjak, A. Prina-Mello, S. Resch, C. Schimpel, I. V. Vrček, E. Wysokińska and H. H. Gorris, *Adv. Healthcare Mater.*, 2019, **8**, e1801233.
- 126 Z. Yu, O. Vepris, C. Eich, Y. Feng, I. Que, M. G. M. Camps, H. Zhang, F. A. Ossendorp and L. J. Cruz, *Mikrochim. Acta*, 2022, **189**, 368.
- 127 A. Gupta, S. Ghosh, M. K. Thakur, J. Zhou, K. Ostrikov, D. Jin and S. Chattopadhyay, *Prog. Mater. Sci.*, 2021, **121**, 100838.
- 128 H. S. Han and K. Y. Choi, *Biomedicines*, 2021, **9**, 305.

